

SYNTHESIS AND CHARACTERIZATION
OF
TETRACARBONYL[N,N'-BIS(FERROCENYLMETHYLENE)
ETHYLENEDIAMINE]MOLYBDENUM(0) COMPLEX

A THESIS SUBMITTED TO
THE GRADUATE SCHOOL OF NATURAL AND APPLIED SCIENCES
OF
MIDDLE EAST TECHNICAL UNIVERSITY

BY

FATMA SANEM KOÇAK

IN PARTIAL FULFILLMENT OF THE REQUIREMENTS
FOR
THE DEGREE OF MASTER OF SCIENCE
IN
CHEMISTRY

MAY 2005

Approval of the Graduate School of Natural and Applied Sciences

Prof. Dr. Canan Özgen
Director

I certify that this thesis satisfies all the requirements as a thesis for the degree of Master of Science.

Prof. Dr. Hüseyin İşçi
Chairman of the Chemistry Department

This is to certify that we have read this thesis and that in our opinion it is fully adequate, in scope and quality, as a thesis for the degree of Master of Science.

Prof. Dr. Saim Özkâr
Supervisor

Examining Committee Members

Prof. Dr. Hüseyin İşçi (METU,CHEM) _____

Prof. Dr. Saim Özkâr (METU,CHEM) _____

Prof. Dr. M.Ahmet Önal (METU,CHEM) _____

Prof. Dr. Ceyhan Kayran (METU,CHEM) _____

Prof. Dr. Yavuz İmamoğlu (Hacettepe Univ.,CHEM) _____

I hereby declare that all information in this document has been obtained and presented in accordance with academic rules and ethical conduct. I also declare that, as required by these rules and conduct, I have fully cited and referenced all material and results that are not original to this work.

Name, Last name: Fatma Sanem Koçak

Signature:

ABSTRACT

SYNTHESIS AND CHARACTERIZATION OF TETRACARBONYL[N,N'-BIS(FERROCENYLMETHYLENE) ETHYLENEDIAMINE]MOLYBDENUM(0) COMPLEX

Koçak, Fatma Sanem

M.S., Department of Chemistry
Supervisor: Prof. Dr. Saim Özkâr

May 2005, 67 pages

In this study a bidentate ligand containing two ferrocenyl moieties, N,N'-bis(ferrocenylmethylene)ethylenediamine, was prepared by condensation reaction of ferrocenecarboxyaldehyde and ethylenediamine on refluxing in benzene. The molecule was identified by IR, Raman, UV-Vis, ^1H -, ^{13}C -NMR spectroscopies. Then, this bidentate molecule was reacted with tetracarbonyl(bicyclo[2.1.1] hepta-2,5-diene)molybdenum(0). The ligand substitution reaction in toluene yielded the new complex, tetracarbonyl[N,N'-bis(ferrocenylmethylene)ethylenediamine]molybdenum(0). This new complex could be isolated from the reaction solution in the form of orange crystals and fully characterized by elemental analysis, IR, UV-Vis, MS, ^1H - and ^{13}C -NMR spectroscopies. As a bidentate ligand, N,N'-bis(ferrocenylmethylene)ethylenediamine binds the metal atom in the two cis positions in the pseudooctahedral geometry of the molybdenum-complex.

Electrochemistry of the tetracarbonyl[N,N'-bis(ferrocenylmethylene)

ethylenediamine]molybdenum(0) was studied by cyclic voltammetry, chronoamperometry and controlled potential electrolysis combined with the UV-Vis or infrared spectroscopy. One irreversible oxidation and three reversible oxidations were observed in the cyclic voltammogram. Irreversible and a reversible oxidations are attributed to molybdenum and the other two reversible oxidation to iron centers. It is found that the two ferrocene groups started communication with each other after formation of molybdenum-complex.

Keywords: Ferrocene, Carbonyl, Molybdenum, Electrochemistry, Ethylenediamine, Diimine.

ÖZ

TETRAKARBONİL[N,N'-BİS(FERROSENMETİLEN) ETİLENDİAMİNE]MOLİBDEN(0) KOMPLEKSİNİN SENTEZİ VE KARAKTERİZASYONU

Koçak, Fatma Sanem
Yüksek Lisans, Kimya Bölümü
Tez Yöneticisi: Prof. Dr. Saim Özkâr

Mayıs 2005, sayfa 67

Bu çalışmada, iki ferrosen birimi içeren ve ikidişli bir ligant olan N,N'-bis(ferrosenilmetilen)etilendiamin molekülü benzende geri soğutucu altında ferrosen karboksaldehit ve etilendiaminin kondenzasyon tepkimesiyle hazırlandı. Molekül IR, ¹H-, ¹³C-, UV-Vis, ve Kütle spektroskopisi teknikleri yardımıyla tanımlandı. Daha sonra, bu ikidişli molekül tetrakarbonil(bisiklo[2.1.1]hepta-2,5-diene)molibden(0) ile tepkimeye sokuldu. Toluende gerçekleştirilen ligant yerdeğiştirme tepkimesi, tetrakarbonil[N,N'-bis(ferrosenilmetilen)etilendiamin]molibden(0) formulündeki yeni kompleksin oluşumu ile sonuçlandı. Bu yeni kompleks çözelti ortamından turuncu kristaller şeklinde izole edilebildi ve element analizi, IR, Raman, UV-VIS, MS, ¹H- ve ¹³C-NMR spektroskopileri ile tam olarak tanımlandı. İkidişli N,N'-bis(ferrosenilmetilen)etilendiamin ligantı, metal atomuna iki cis konumundan bağlanarak görünürde oktahedral geometriye sahip olan molibden kompleksini oluşturdu.

Tetrakarbonil[N,N'-bis(ferrosenilmetilen)etilendiamin]molibden(0) kompleksinin elektrokimyası dönüşümlü voltametri, UV-VIS ve IR spektroskopileri

ile kombine edilmiş sabit potansiyel elektrolizi ve kronoamperometri ile çalışıldı. Dönüşümlü voltametrde bir tersinmez ve üç tersinir yükseltgenme gözlendi. Bunlardan tersinmez olan ve tersinir yükseltgenmelerden biri molibdene, diğer iki tersinir yükseltgenmenin de merkez demir atomlarına ait olduğu gözlendi. Molibden kompleksinin oluşmasından sonra, iki ferrosen grubunun birbiri ile elektronik iletişime geçtikleri bulundu.

Anahtar Kelimeler: Ferrosen, Karbonil, Molibden, Elektrokimya, Etilendiamin, Diimin.

To my family

ACKNOWLEDGMENTS

I would like to express my sincere gratitude to Prof. Dr. Saim Özkâr for his encouragement, never ending support and supervision throughout in this study.

I would like to extend my gratitude to Prof. Dr. M. Ahmet Önal for his close interest and valuable criticism in the electrochemistry part of this work.

I also would like to thank to Prof. Dr. Levent Aksu and his assistance Hüseyin Çelikkán for their help in chronoamperometric study.

I am indebt to Taner Atalar for giving me moral support and valuable advices.

I would like to thank Ercan Bayram, Önder Metin, Pelin Erdiñç, Ceyhun Akyol, Fatma Alper, Cüneyt Kavaklı, Mehmet Zahmakıran, Murat Rakap, Dilek Ayşe Boğa, and Ezgi Keçeli, for their caring and their encouragement during my study.

TABLE OF CONTENTS

PLAGARISM.....	iii
ABSTRACT.....	iv
ÖZ.....	vi
ACKNOWLEDGEMENTS.....	ix
TABLE OF CONTENTS.....	x
LIST OF TABLES.....	xii
LIST OF FIGURES.....	xiii
CHAPTERS	
1. INTRODUCTION.....	1
2. BONDING.....	9
2.1. Metal-Carbonyl Bonding.....	9
2.2. Metal-Imine Bonding.....	11
3. EXPERIMENTAL.....	17
3.1. Basic Techniques.....	17
3.2. Infrared Spectra.....	20
3.3. NMR Spectra.....	20
3.4. Mass Spectra.....	20
3.5. Raman Spectra.....	20
3.6. Elemental Analysis.....	20
3.7. UV-Vis Spectra.....	21
3.8. Cyclic Voltametry.....	21
3.9. In-Situ constant Potential/ Current Electrolysis.....	22
3.10. Synthesis of Ligand and Complexes.....	23
3.10.1. Synthesis of the Mo(CO) ₄ (bicyclo[2.1.1] hepta-2,5-diene).....	23
3.10.2. Synthesis of the Mo(CO) ₄ ($\eta^{2:2}$ -1,5-cyclooctadiene)	24
3.10.3. Synthesis of the N,N'-Bis(ferrocenylmethylene)ethylenediamine..	24

3.10.4. Synthesis of the Tetracarbonyl[N,N'-bis(ferrocenylmethylene) ethylenediamine]molybdenum(0), Mo(CO) ₄ (BFEDA).....	25
4. RESULT AND DISCUSSION.....	26
4.1. N,N'-Bis(ferrocenylmethylene)ethylenediamine, BFEDA	26
4.2. Mo(CO) ₄ [N,N'-Bis(ferrocenylmethylene)ethylenediamine].....	34
4.3. Electrochemistry of BFEDA and Mo(CO) ₄ (BFEDA).....	46
5. CONCLUSION.....	62
REFERENCES.....	64
APPENDIX.....	67

LIST OF TABLES

TABLES

4.1. Changes in chemical shifts for α , β and C_5H_5 positions relative to ferrocene (4.19 ppm).....	31
4.2. The electronic absorption bands of free ferrocene.....	33
4.3. The CO stretching frequencies of complexes having $Mo(CO)_4$ moiety ($in\ cm^{-1}$) as observed in the IR spectra taken from toluene solution.....	37
4.4 CO stretching frequencies and ^{13}C -NMR chemical shifts (δ , ppm) of the carbonyl groups of $Mo(CO)_4(L)_2$ complexes with three different ligands.....	42
4.5. ^{13}C -NMR chemical shifts (δ , ppm) belonging to carbonyl groups of $M(CO)_4(L)_2$	42
4.6. ^{13}C -NMR chemical shifts (δ , ppm) belonging to carbonyl groups of $Mo(CO)_5L$	42
4.7. The result of Elemental analysis for the complex $Mo(CO)_4(BFEDA)$	43
4.8. The absorption wavelengths (λ_{max}) of free ferrocene and free ferrocenium ion in nm.....	56
4.9. Spectral change in UV-VIS of (a) BFEDA and (b) $Mo(CO)_4(BFEDA)$ during controlled potential electrolysis in CH_2Cl_2 and TBATFB solution.....	58

LIST OF FIGURES

FIGURES

1.1. The structure of the ferrocene suggested initially by Kelly and Pauson.....	3
1.2. The structure of ferrocene as determined by single crystal X-ray diffraction..	3
1.3. Suggested structural formula of BFEDA.....	6
1.4. Suggested structural formula of Mo(CO) ₄ (BFEDA).....	6
1.5. Ligand substitution reaction of bicyclo[2.1.1] hepta-2,5-diene (NBD) in Mo(CO) ₄ (η ^{2:2} -NBD) with N,N'-bis(ferrocenylmethylene)ethylenediamine at room temperature in toluene.....	7
2.1. Molecular orbital description of metal-carbonyl interaction.....	10
2.2. Resonance Hybrids of metal-carbonyl bond.....	10
2.3. Competition for π-bonding in metal-carbonyl derivatives.....	11
2.4. The structure of an imine molecule.....	11
2.5. The molecular orbital diagram of an imine molecule.....	12
2.6. Molecular orbital description of the metal-imine bonding.....	13
2.7. Polarization of the π-bond in an imine molecule.....	14
2.8. Nucleophilic attack of water molecule to an imine molecule.....	14
2.9. Schematic representation of molecular-orbital diagram metal-imine π-bonding.....	15
2.10. A nucleophile attacks the nitrogen atom of the coordinated imine.....	16
3.1. Nitrogen gas purification steps.....	18
3.2. Standard schlenk tube.....	18
3.3. Experimental set up for the BFEDA synthesis.....	19
3.4. Cyclic voltammetry cell.....	21

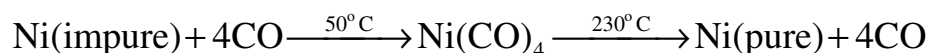
3.5. The apparatus used for measuring in-situ spectral changes during the constant potential and constant current electrolysis at 0 °C temperature.....	22
3.6. The cell used for measuring in-situ spectral changes during the constant potential electrolysis at room temperature.....	23
4.1. IR spectrum of the BFEDA in CH ₂ Cl ₂	27
4.2. Representation of stretching modes in BFEDA	27
4.3. Infrared spectrum of BFEDA taken from KBr disc.....	28
4.4. Raman spectrum of the BFEDA in solid form.....	28
4.5. Suggested structural formula of BFEDA	29
4.6. ¹ H-NMR spectrum of BFEDA in CDCl ₃	30
4.7. ¹³ C- ¹ H-NMR spectrum of the BFEDA in CDCl ₃	32
4.8. The UV-VIS spectrum of the BFEDA in CH ₂ Cl ₂	33
4.9. IR spectrum of the solution taken in toluene during the reaction of Mo(CO) ₄ (η ^{2,2} -NBD) with BFEDA.....	36
4.10. Symmetry coordinates for the CO stretching vibration modes in the cis-M(CO) ₄ L ₂	37
4.11. ¹ H-NMR spectrum of Mo(CO) ₄ (BFEDA) in CD ₂ Cl ₂	39
4.12. The ¹ H-NMR spectrum of Mo(CO) ₄ (BFEDA) in CD ₂ Cl ₂ , the 5.50-3.50 ppm region expanded.....	39
4.13. ¹³ C- ¹ H-NMR spectrum of the Mo(CO) ₄ (BFEDA) in CD ₂ Cl ₂	41
4.14. Molecular peak of Mo(CO) ₄ (BFEDA) in mass spectrum.....	44
4.15. Mass spectrum of Mo(CO) ₄ (BFEDA).....	45
4.16. UV-VIS spectrum of Mo(CO) ₄ (BFEDA) in CH ₂ Cl ₂	46
4.17. CV of BFEDA in CH ₂ Cl ₂ solution containing TBABF ₄ as supporting electrolyte.....	47
4.18. CV of 1×10 ⁻⁴ M solution of Mo(CO) ₄ (BFEDA) in CH ₂ Cl ₂ containing tetrabutylammonium tetrafluoroborate.....	48
4.19. Differential pulse voltammogram of Mo(CO) ₄ (BFEDA).....	49
4.20. CV of Mo(CO) ₄ (BFEDA) at a scan rate 50 mV/s with reference electrode of Ag-wire and SCE.....	50
4.21. CV of Mo(CO) ₄ (BFEDA) at scan rates of 50, 100, 200,500 and 1000 mV/s in CH ₂ Cl ₂ with reference electrode of Ag-wire.....	51

4.22. Graph of peak current (I_p) versus square root of scan rates ($v^{1/2}$).....	52
4.23. CV of $\text{Mo}(\text{CO})_4(\text{BFEDA})$ with UME electrode.....	54
4.24. Chronoamperometric study of $\text{Mo}(\text{CO})_4(\text{BFEDA})$ using UME.....	54
4.25. UV-VIS monitored controlled potential electrolysis of BFEDA in CH_2Cl_2 and 0.015 M TBATFB solution.....	55
4.26. UV-VIS monitored constant current electrolysis of $\text{Mo}(\text{CO})_4(\text{BFEDA})$ until two electron oxidations were completed.....	57
4.27. UV-VIS monitored controlled potential electrolysis of $\text{Mo}(\text{CO})_4(\text{BFEDA})$	58
4.28. FTIR spectra during electrolysis of 1×10^{-4} M $\text{Mo}(\text{CO})_4(\text{BFEDA})$ in CH_2Cl_2 and 0.1 M TBATFB solution at constant current.....	61

CHAPTER 1

INTRODUCTION

In historical terms the carbon-transition metal bond is quite old. The first transition metal-ethylene complex $K[PtCl_3(C_2H_4)]$ was discovered by Zeise in 1827 but a whole century passed before the real significance of this compound was understood. From an industrial stand point of view, the first applications of organometallic chemistry date from discovery of nickel-tetracarbonyl by Langer and Mond in 1888. The application of this compound was understood much more rapidly and crude nickel has been refined by Mond carbonylation-decarbonylation process for many decades.¹



The great postwar breakthrough occurred in 1951, when bis(cyclopentadienyl)iron or 'ferrocene' appeared in famous Nature article published by Kealy and Pauson. After the discovery of ferrocene, organometallic chemistry has achieved explosive development. The barrier between organic and inorganic chemistry was eliminated. As a result, important concepts such as π -back bonding, agostic interaction, β -hydrogen elimination, reductive elimination, insertion etc have been introduced into the field of chemistry.

Organometallic compounds are generally defined as compounds having at least one metal-carbon bond. However, some compounds that do not contain any metal-carbon bonds such as zero valent metal complexes, hydrides and dinitrogen

complexes are also admitted as member of organometallic compounds because of their close relationship.²

Almost all of the transition metals form compounds in which carbon monoxide acts as a ligand. There are three points of interest with respect to these compounds: (1) Carbon monoxide is not ordinarily considered as a very strong Lewis base and yet it forms strong bonds to the metals in these complexes; (2) the metals are always in a low oxidation state, most often formally in an oxidation state of zero, but sometimes also in a low positive or negative oxidation state; and (3) the 18-electron rule is obeyed by these complexes with remarkable frequency, perhaps 99 % of the time.³ Although in recent years ¹³C-NMR spectroscopy has become increasingly valuable, it is still true that infrared (IR) spectroscopy is the preeminent physical method for characterizing metal-carbonyls.⁴ In infrared spectroscopy the stretching vibration of C=O bond appears at 1700-2100 cm⁻¹, a region usually free of other ligand vibrations. The intensity is high because of the large dipole moment change during the vibration, thanks to the polarization of the CO on binding to the metal. In complexes with more than one CO, the carbonyls do not usually vibrate independently, but instead vibrate in concert, and are therefore said to be coupled together in a way that depends on the symmetry of the M(CO)_n fragment.⁵

In addition to the well-known carbonyl ligands, molecules containing the >C=N- imine group have played a major role in development of contemporary coordination chemistry as well. The π-acceptor imine ligands bind to metal having low oxidation state through nitrogen atom.⁶

The ferrocene, which is a landmark in the development of organometallic chemistry, was first synthesized and characterized approximately fifty years ago. In 1948 Miller, Tebboth, and Tremaine, attempting to synthesize amines from olefines and nitrogen in the presence of iron catalysts, found that with cyclopentadiene, an iron- containing compound was formed, FeC₁₀H₁₀. Three years later, Kealy and Pauson obtained the same compound in an attempt to oxidize C₅H₅MgBr with FeCl₃

and, in analogy to main group element alkyls, suggested a structure with two metal-carbon σ -bond (Figure 1.1):

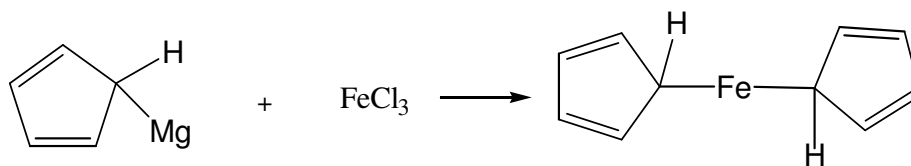


Figure 1.1. The structure of the ferrocene suggested initially by Kelly and Pauson.

The true nature of this remarkably stable product was recognized independently by G. Wilkinson, R.B. Woodward and E.O. Fischer who suggested a sandwich or double-cone structure (Figure 1.2).

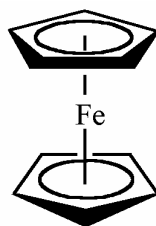


Figure 1.2. The structure of ferrocene as determined by single crystal X-ray diffraction.

The ferrocene behaves much like a three-dimensional arene. For example it undergoes Friedel-Crafts acylation like a benzene derivative. However, in contrast to benzene, ferrocene is sensitive to oxidation and the ferrocenium cation, Cp_2Fe^+ , paramagnetic 17-electron specie, is readily formed in the presence of various oxidants.⁷

The study of ferrocene derivatives has increased exponentially during the last decades due to their applications in wide variety of areas, including catalysis, organic synthesis and design of new materials. Ferrocene derivatives containing atoms with good donor abilities have attracted additional interest, since the coordination of a

metal to these heteroatoms produces multicenter molecules in different environments which may influence the mutual cooperation of these metals in a variety of processes.⁸ Ferrocene has become a versatile building block for the synthesis of compounds tailor-made properties in many fields, such as organic synthesis, homogeneous catalysis, materials chemistry, and production of fine chemicals, due to its high stability and powerful electron releasing ability and well-established methods for its incorporation into more complex structures.¹⁵ In general, three properties distinguish ferrocenyl substituents from other, purely organic moieties: (i) unique steric bulk with special steric requirements due to the cylindrical shape, (ii) electronic stabilization of adjacent electron-deficient centers due to participation of the iron atom in the dispersal of the positive charge, and (iii) chemical stability and reversibility of the ferrocene/ferrocenium⁺ redox couple, which has made ferrocene one of the most classical redox agents of the organometallic chemistry.⁹ Ferrocene have been used in the synthesis of many new materials having interesting properties. For instance, molecules containing ferrocene moiety have been used as homogenous catalysts, molecular sensors, non-linear optic materials, liquid crystals, biosensors and photo-catalysts.^{10, 11, 12} Besides of that, some examples of antitumor materials containing ferrocenyl groups have also been reported.⁸

In particular, the relatively high electron-transfer rates of metallocenes make their incorporation into redox catalyst attractive. Such ligands may enhance electron transfer properties of catalysts as well as act as electron-storage devices.¹³ From a redox viewpoint, ferrocene derivatives are interesting monoelectron reservoir complexes capable of acting as mediators in redox-catalytic reactions. An important challenge in this field is the design and synthesis of multielectron redox mediators, which could transfer electrons simultaneously at the same potential. Each of these redox centers should then be far enough from one another to have the same redox potential and still close enough to each other to provide all electrons at substrate site. Transition metal compounds containing ferrocene based ligands, such as 1,1'-bis(diphosphino)ferrocene, often show superior catalytic activity when compared to complexes containing other types of bidentate diphosphino ligands.¹⁴ This unusual

catalytic activity is likely because of the availability of different but cooperatively conjugated metal sites and the unique opportunity to control the chemical, physico-chemical and structural variations in coordination sphere of the central transition metal fragment through change of the oxidation state of the remote ferrocene subunits.¹⁵

As part of an ongoing interest in transition metal compounds with electronically communicating metal centers linked by conjugated bridges, we thought that the Group 6 metal-carbonyl complexes of a ferrocene-functionalized imine ligand would be of interest for studying the long-range metal-metal interactions. The N,N'-bis(ferrocenylmethylene)ethylenediamine (BFEDA) was used as a bidentate imine ligand which can bind a transition metal through two nitrogen atoms. The BFEDA molecule has two ferrocenyl moieties. Since the two ferrocene groups are isolated from each other (i.e. no electronic interaction) and equivalent, this ligand can be considered as a two-electron reservoir. However, when the molecule is coordinated to a transition metal, e.g. molybdenum, with π -bonding there might exist an electronic communication between the iron and the transition metal atoms, and, thus, between the ferrocenyl groups. The metal-imine bonds provide π -conjugation between molybdenum and ferrocene moieties. The tetracarbonyl[N,N'-bis(ferrocenylmethylene)ethylenediamine]metal(0) complexes of the Group 6 elements have been considered as model molecules, having three redox active centers which are electrically communicating with each other. In other words, the metal centers are expected to oxidize at different potentials. In this study, we synthesized and characterized the N,N'-bis(ferrocenylmethylene)ethylenediamine, (BFEDA), (Figure 1.3), and its corresponding tetracarbonyl-molybdenum complex (Figure 1.4). The chromium analogue has already been studied by another researcher in our group.¹⁶

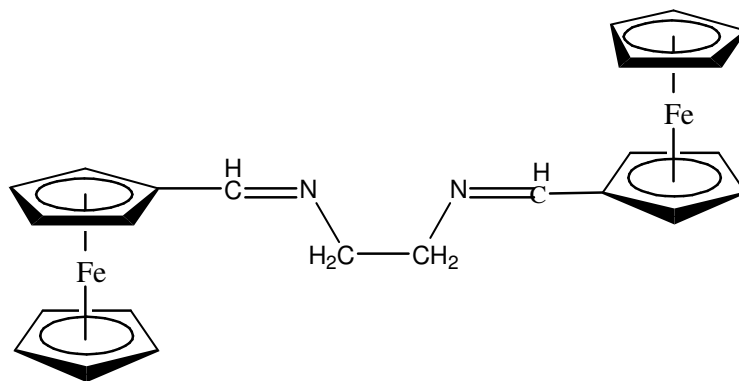


Figure1.3. Suggested structural formula of BFEDA

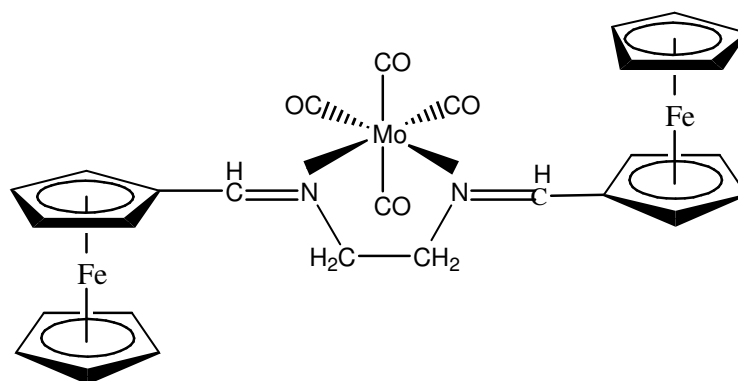


Figure 1.4. Suggested structural formula of $\text{Mo}(\text{CO})_4(\text{BFEDA})$

First, the BFEDA was synthesized by refluxing the ferrocenecarboxaldehyde with ethylenediamine. Then $\text{Mo}(\text{CO})_4(\text{BFEDA})$ complex was synthesized by substitution of bicyclo[2.1.1]hepta-2,5-diene (NBD) in $\text{Mo}(\text{CO})_4(\eta^{2:2}\text{-NBD})$ at room temperature in toluene.

The tetracarbonyl(η^4 -diene)metal(0) complexes of group 6 elements have been known for over three decades and used as $\text{M}(\text{CO})_4$ transfer reagents to prepare a variety of $\text{M}(\text{CO})_4\text{L}_2$ compounds.¹⁷ Tetracarbonyl($\eta^{2:2}$ -1,5-cyclooctadiene)metal(0) and tetracarbonyl(bicyclo[2.1.1]hepta-2,5-diene)metal(0) complexes are the well

known $M(CO)_4$ transfer reagents in synthesis of many transition metal complexes due to lability of M-diene bond.¹⁸

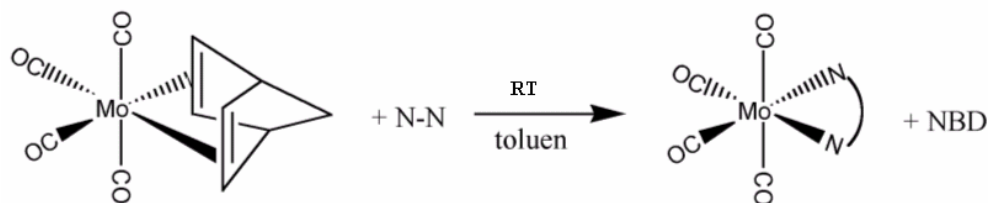


Figure.1.5. Ligand substitution reaction of bicyclo[2.1.1] hepta-2,5-diene (NBD) in $Mo(CO)_4(\eta^{2:2}\text{-NBD})$ with N,N'-bis(ferrocenylmethylene)ethylenediamine at room temperature in toluene.

In addition, $Mo(CO)_4(\text{BFEDA})$ complex was also obtained from thermal substitution of 1,5-cyclooctadiene in $Mo(CO)_4(\eta^{2:2}\text{-COD})$ by BFEDA. The complex was isolated from the reaction solution by crystallization and characterized by means of elemental analysis, UV-VIS, IR, NMR and Mass spectroscopy techniques. The electrochemical behavior of $Mo(CO)_4(\text{BFEDA})$ was studied by using cyclic voltammetry and the mechanisms of electrode reactions were investigated by in-situ UV-VIS, chronoamperometry and IR spectroscopic measurements.

Electrochemistry was used first in the field of organometallic chemistry to generate some metastable organometallic compounds in solution.¹⁹ But, later electrochemistry has been used to examine the electronic structure of organometallic compounds and to study their redox behavior. A full band detailed understanding of the electron transfer properties of organometallic complexes can be achieved only by a combination of spectroscopic and electrochemical studies. For example, the combination of the UV-visible electronic absorption spectroscopy and the cyclic voltammetry can give additional useful information about the electronic structure of the organometallic compounds.²⁰

Cyclic voltammetry is a technique where the cell current is recorded as a function of the potential of the working electrode. The potential of the working electrode is varied at a constant rate backward and forwards between two limits, which lie within the voltammetric range for the solution under study.²¹ Cyclic voltammetry is used for the determination of the redox behavior of organometallic compounds and it is an important tool in order to study the oxidation and reduction behavior of organometallic compounds, because it is a rapid instrumental technique to determine electrode potential and to investigate the reversibility of electron transfer reaction.²² Differential pulse voltammetry differs from that of cyclic voltammetry due to their application of potential. In former technique, potential is applied like stairs between two limits. Differential pulse voltammetry gains greater sensitivity by taking advantage of the fact that a small jump in potential has a much greater effect on analytical signal.

In order to determine the number of electrons involved at the reduction or oxidation peaks in the cyclic voltammograms, the controlled potential coulometry was used. The changes in solution during the process followed by UV-VIS spectroscopy. In controlled potential electrolysis the potential of the working electrode is held at a fixed potential on the plateau of a voltammetric wave, and the electroactive species is oxidized or reduced completely.²¹

CHAPTER 2

BONDING

2.1. Metal-Carbonyl Bonding

The carbon monoxide does not form particularly stable complexes with BF_3 or with main group metals such as potassium or magnesium. Yet transition metal complexes with carbon monoxide are known by the thousand. The CO ligands are bound to metal through the carbon atom and the complexes are called as metal carbonyls. Furthermore, the metals occur most usually in low formal oxidation states.

The bonding of CO to a metal can be described in terms of two synergic components; the more σ -donation by the carbonyl, the stronger π -back-bonding by the metal:

- i) σ -dative bonding: Two electron donation of the lone pair on carbon into a vacant metal d-orbital; This electron donation makes the metal more electron rich and in order to compensate for this increased electron density, a filled metal d-orbital may interact with empty π^* -orbital on the carbonyl ligand to relieve itself of the added electron density.
- ii) π -back-bonding: Effective overlap of the metal d-orbital and carbon monoxide π^* -orbital results in an extensive back bonding. These interactions are shown diagrammatically in Figure 2.1.

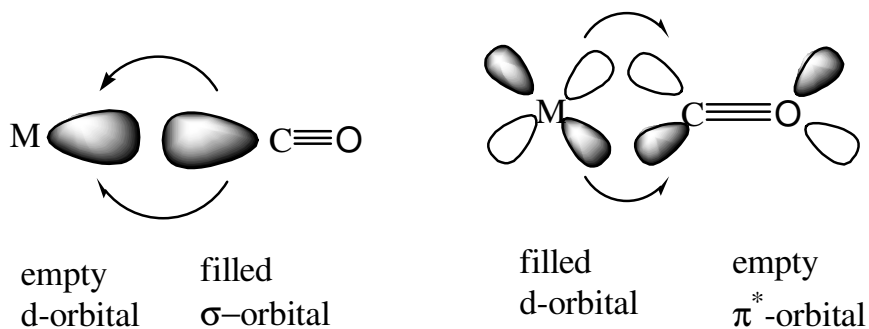


Figure 2.1. Molecular orbital description of metal-carbonyl interaction

Valence bond resonance hybrids lead a similar description and indicate a metal-carbon bond order being greater than one and a C-O bond order being less than three (Figure 2.2)

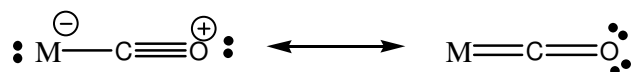


Figure 2.2. Resonance Hybrids of metal-carbonyl bond

Since π -back bonding depends crucially on the electron density of the metal, it does not only strengthens the M-CO bond, but also provides a very sensitive probe for the electronic characteristics of the metal center. Extensive back bonding in electron rich complexes lowers the CO stretching frequency. This is consistent with the bonding model, an increase in the electron density on the metal atom is delocalized over the CO ligands, by populating the carbonyl π^* -orbital thus weakening the CO bond. Nevertheless, the converse is true if the complex is positively charged. Also other strong σ -donor and π -acceptor ligands attached trans to CO ligand in a mixed metal ligand carbonyl weakens M-CO bond and strengthen C \equiv O bond simultaneously.²³ This weakening or strengthening is due to the sharing of the same d-orbital by the carbonyl and the L- ligand, trans to that carbonyl (π -competition) (Figure 2.3)

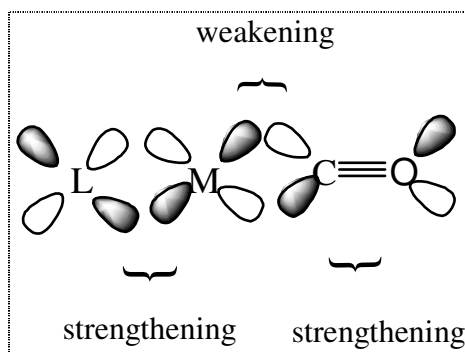


Figure 2.3. Competition for π -bonding in metal-carbonyl derivatives

2.2.Metal-Imine Bonding

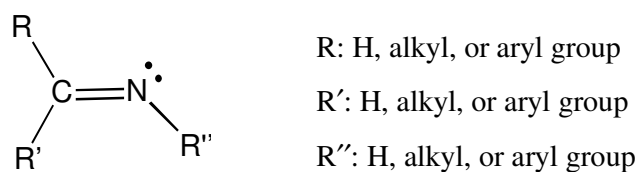


Figure 2.4. The structure of an imine molecule

Carbon-nitrogen double bond in an imine molecule consists of a σ - bond and a π - bond as shown in Figure 2.4. In the MO energy level diagram there will be two σ - orbitals (bonding and antibonding) and two π -orbitals (bonding and antibonding) for C=N: moiety (Figure 2.5). The bonding orbitals are mainly localized on the nitrogen atom, while antibonding orbitals belong mainly to the carbon atom, considering the fact that nitrogen is more electronegative than carbon. Moreover, there should be one nonbonding σ -orbital localized on the nitrogen atom because there are two lone-pair electrons on the nitrogen atom as seen from the structure of the molecule. Totally six electrons (2 from the carbon and 4 from the nitrogen) are available to occupy molecular orbitals of the C=N: moiety of the imine molecule.

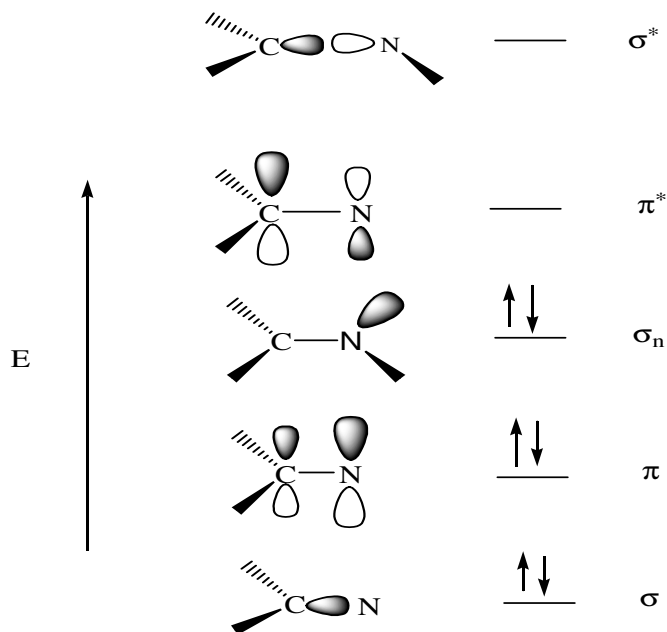


Figure 2.5. The molecular orbital diagram of an imine molecule

The HOMO of the imine molecule is the sp^2 nonbonding orbital on nitrogen, and the LUMO is the antibonding π^* orbital. A strong σ interaction between metal and the imine ligand should be expected because the HOMO completely localized on the nitrogen, is directed to the $d\sigma$ orbital of the metal along the bond-axis (Figure 2.6.a). On the other hand, the π bonding takes place to the lower extent in comparison with the σ -bonding because the π^* orbital (LUMO) of imine is mainly localized on the carbon atom, that is, the LUMO has its smaller amplitude on the nitrogen (Figure 2.6.b).

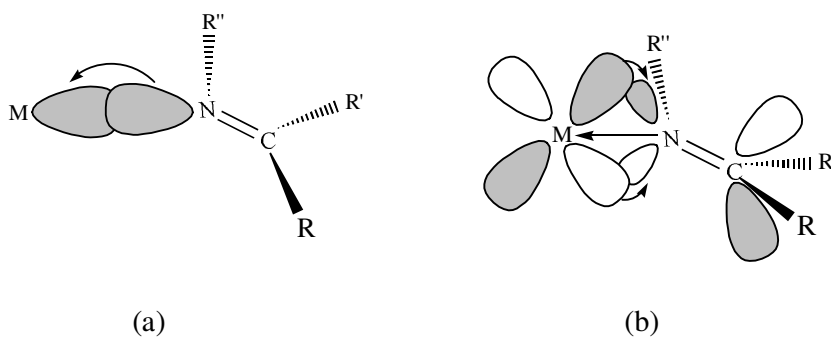


Figure 2.6. Molecular orbital description of the metal-imine bonding

(a) Metal \leftarrow imine σ bonding; electrons are donated from nonbonding sp^2 orbital on the nitrogen atom to the empty d orbital of the metal.

(b) Metal \rightarrow imine π bonding; the electrons on the $d\pi$ orbital of the metal are backdonated to the empty π^* orbital of the imine.

These σ and π interactions are synergic. If the π^* orbital of the imine molecule were mainly localized on the nitrogen atom, π bonding would have been much stronger; i.e. imines would have π -accepting ability as strong as the CO ligand. However, the imine ligand is a strong σ -donor and weak π -acceptor, depending on the substituents on the carbon and nitrogen atoms, transition metal and the other ligands coordinated to the metal.

In an imine molecule the more electronegative nitrogen atom strongly attracts the electrons of the σ bond and the π bond causing the C=N bond highly polarized; the carbon atom bears a partial positive charge and the nitrogen atom bears a partial negative charge. Polarization of the π -bond can be represented by the following resonance structures:

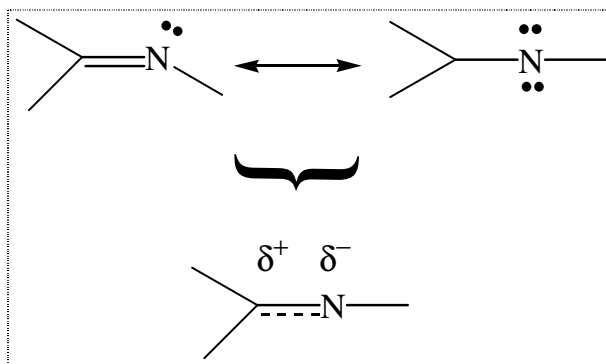


Figure 2.7. Polarization of the π -bond in an imine molecule

The nucleophile, which is electron-rich, attacks on the carbon atom bearing a positive charge. For example, highest occupied molecular orbital of the water molecule, which acts as a nucleophile attacks to imine molecule toward LUMO of the imine molecule, which is mainly localized on the carbon atom.

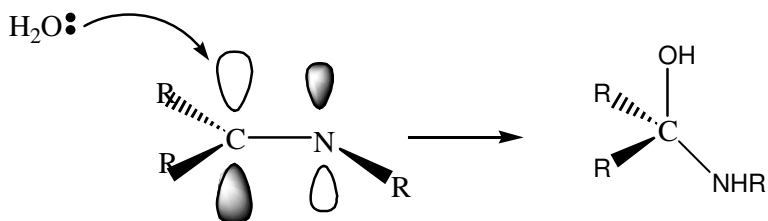


Figure 2.8. Nucleophilic attack of water molecule to imine molecule.

In π -bonding of imine with metal atom, the three molecular orbitals resulting from the overlap of the three atomic orbitals are shown in Figure 2.9.

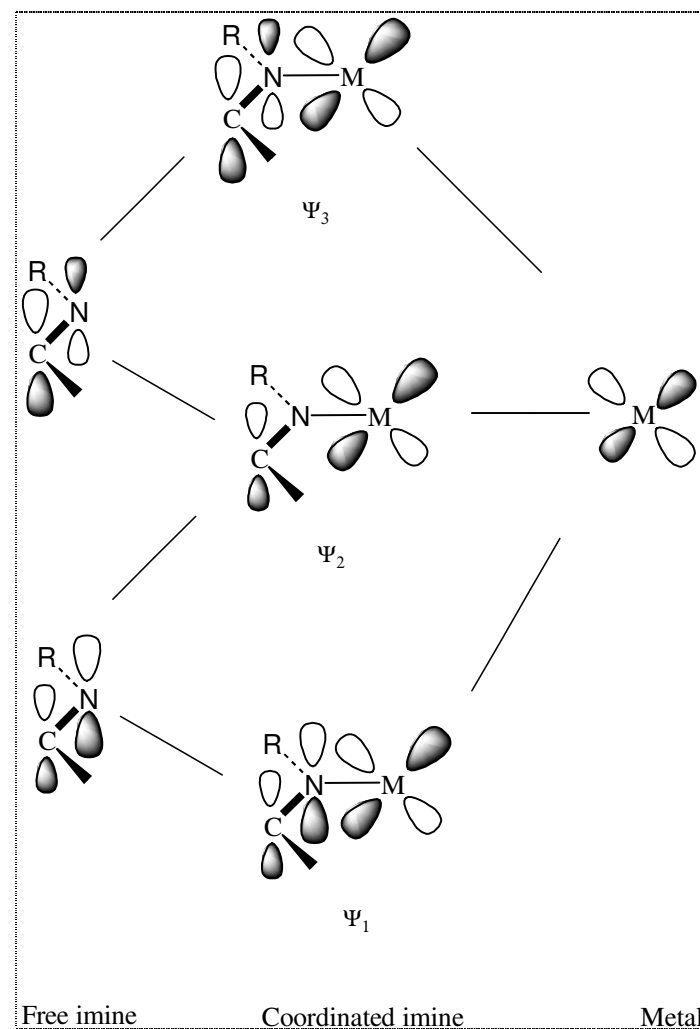


Figure 2.9. Schematic representation of molecular orbital diagram metal-imine π -bonding

The molecular orbitals Ψ_1 and Ψ_2 are filled. The important orbital is Ψ_2 which is derived from the old π^* level of the orbital. Placing the electron density within Ψ_2 orbital results in a building-up of the electron density in the π -symmetry orbitals on the carbon atom of the imine. This will result in a repulsion being experienced by any incoming nucleophile, and a deactivation of the imine towards nucleophilic attack. It is generally found that imines are stabilized by coordination to a π -bonding transition metal. The balance between stabilization and the activation of the imine

towards hydrolysis depends on the relative polarization of the ligand and the back donation from the metal. Many factors involved (charge on metal, charge on ligand, back-donation, and configuration of ligands) are interdependent and finely balanced. The formation of a chelated imine complex is an important factor, but once again examples are known in which chelated ligands are both activated and deactivated towards hydrolysis.²⁴ In general, the greater the thermodynamic stability of the imine complex, the smaller the tendency towards hydrolysis. However, they might undergo a nucleophilic attack on the nitrogen atom bearing a partial positive charge as long as the transition metal and the substituent on the nitrogen do not create a significant steric crowding as shown in Figure 2.10.⁹

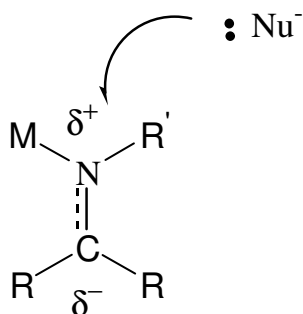


Figure 2. 10. A nucleophile attacks the nitrogen atom of the coordinated imine.

CHAPTER 3

EXPERIMENTAL

3.1. Basic Techniques

Most of the organometallic compounds are air sensitive and tend to decompose if not handled properly. Those compounds can be oxidized easily, especially when they are in solution, because of their sensitivity to oxygen and water. Consequently, handling of organometallic compounds should be carried out under dry and deoxygenated atmosphere or under vacuum.

In order to achieve such an atmosphere, an inert gas line, in which oxygen-free dry dinitrogen passes, have been used. Circulated nitrogen gas passes through some purification steps as shown in Figure 3.1. Firstly the inert gas passes through a catalyst (BASF R3.II, Ludwigshafen, Germany) where it is deoxygenated. The catalyst is heated up to 120°C to be regenerated. Then it passes through dried molecular sieves to be removed from its moisture, and finally through glycerine to bubble the flowing gas.

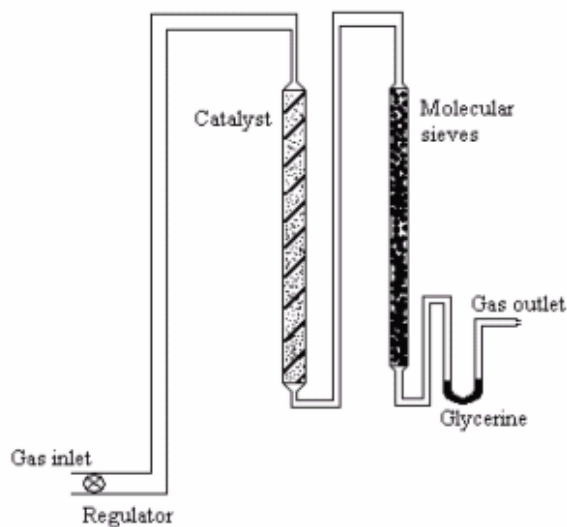


Figure 3.1. Nitrogen gas purification steps

The other fundamental techniques that were used in this study are:

- (i) Schlenk Technique: A Schlenk tube (Figure 3.2) is a flask that has at least one arm where inert gas can be introduced. Usually a three- or two-way stopcock is fitted at the end of the arm. In use, the air in a Schlenk flask should be replaced at least three times by inert gas using a pump and fill procedure and all subsequent handling should be carried out under nitrogen flow.

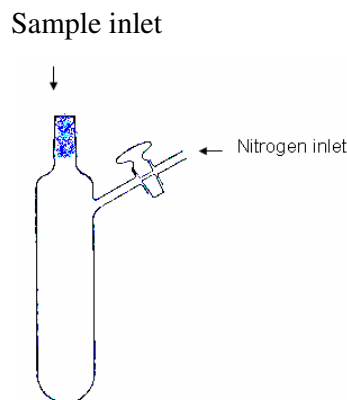


Figure 3.2. Standard schlenk tube

- (ii) Vacuum Line Technique: This technique is used to remove any solvent under low vapor pressure. The tube used for this technique should be trapped in liquid nitrogen.

Solvents used were purified and solvated oxygen was removed by refluxing over a suitable water holder under nitrogen atmosphere for 3 to 4 days before use.

All solvents, ferrocenecarboxaldehyde, were purchased from Aldrich. Ethylenediamine was purchased from Merck.

In synthesis of BFEDA molecule a Dean-Stark apparatus is used to remove water molecules from refluxing solvent. (Figure 3.3)

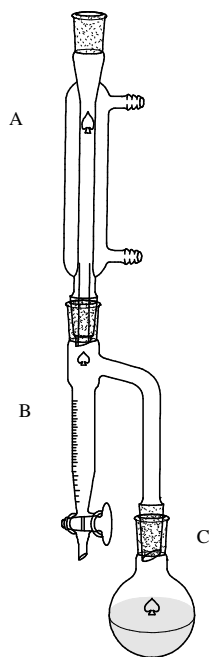


Figure 3.3. Experimental set up for the BFEDA synthesis; A: Condenser, B: Dean-Stark apparatus, C: Round bottom flask.

3.2. Infrared Spectra

The infrared spectra of both the BFEDA and the $\text{Mo}(\text{CO})_4(\text{BFEDA})$ complex were recorded from their dichloromethane or toluene solutions by using a Specac IR-Liquid cell with CaF_2 windows on a Nicolet 510 FTIR Spectrometer instrument with Omnic software. The solid infrared spectrum of BFEDA was taken from its KBr disc.

3.3. NMR Spectra

The ^1H -NMR and ^{13}C -NMR spectra of the BFEDA were taken from their d-chloroform solutions on a Bruker-Spectrospin DPX 400 Ultrashield NMR Spectrometer with Avance software.

3.4. Mass Spectra

FAB-MS was taken on a Fisons VG Autospec with m-nitrobenzylalcohol as matrix at Colorado State University, Fort Collins, USA.

3.5. Raman Spectra

The Raman spectrum of the BFEDA in solid form was recorded by using a Bruker FRA 106/S Spectrometer with Opus software.

3.6. Elemental Analysis

Elemental analysis was carried by using LECO CHNS-932 instrument in the METU Control Laboratory.

3.7. UV-VIS Spectra

The UV-VIS spectra of the ligand and the complex were taken from their CH_2Cl_2 solutions at room temperature on a Hewlett Packard 8452A Model Diode Array Spectrophotometer with UV-Visible ChemStation software.

3.8. Cyclic Voltammetry

The electrochemical experiments of the BFEDA and the $\text{Mo}(\text{CO})_4(\text{BFEDA})$ complex were carried out by the use of CH Instruments 660B electrochemical analyzer and BAS C cell (Figure 3.4). The measurements were repeated with HEKA IEEE 488 model potentiostat.

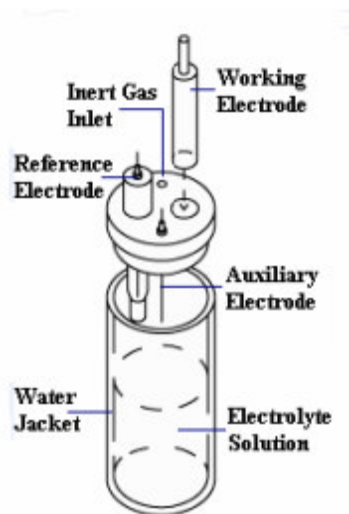


Figure 3.4. Cyclic voltammetry cell

Anhydrous base electrolyte (supporting electrolyte) tetrabutylammonium tetrafluoroborate, $(\text{n-Bu})_4\text{NBF}_4$ was used in order to keep the cell resistance low and suppress the electrical migration current which would exist in the absence of a large concentration of non-reducible cation.

In general, in order to avoid the interference of the reduction waves of oxygen with the waves obtained from compounds, nitrogen gas is allowed to pass

through solution before recording. The surface of the solution is blanketed by nitrogen gas during recording to prevent the re-entry of oxygen.

3.9. In-Situ constant Potential/ Current Electrolysis

In order to determine the number of electrons involved at the reduction or oxidation peaks present, coulometric analysis were carried out in a cell shown in Figure 3.5. Oxidation and reduction processes of the BFEDA and the $\text{Mo}(\text{CO})_4(\text{BFEDA})$ complex were carried out at 0°C in their CH_2Cl_2 solution at the peak potentials observed in cyclic voltammetry. The electrolysis was followed by taking the electronic absorption spectra in every 5 mC by using a Hewlett Packard 8452A Model Diode Array Spectrophotometer. The electrolysis was also followed by taking IR spectra in every 5 mC by using 510 FTIR Spectrometer instrument with Omnic software. The cell, which was used for electrolysis followed by IR spectra, is given in Figure 3.6.

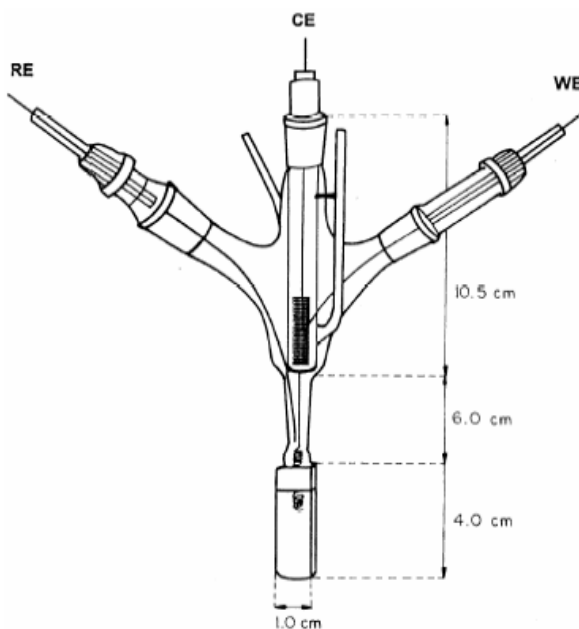


Figure.3.5. The apparatus used for measuring in-situ spectral changes during the constant potential and constant current electrolysis at 0°C temperature; RE: Ag-wire reference electrode; CE: Pt-sieve counter electrode; WE: Pt-wire working electrode.

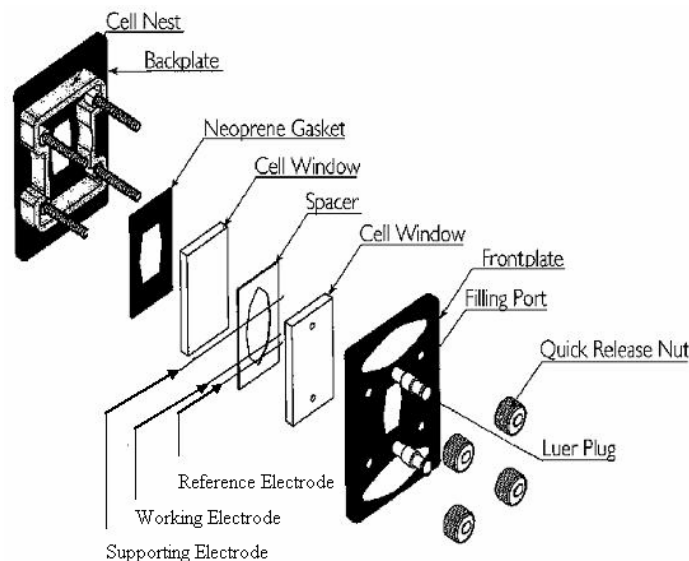


Figure 3.6. The cell used for measuring *in-situ* spectral changes during the constant potential electrolysis at room temperature; Reference Electrode: Ag-wire reference electrode; Supporting Electrode: Pt-sieve counter electrode; Working Electrode: Pt-wire working electrode.

3.10. Synthesis of Ligand and Complexes

3.10.1. Synthesis of the $\text{Mo}(\text{CO})_4(\text{bicyclo}[2.1.1] \text{ hepta-2,5-diene})$

Tetracarbonyl(bicyclo[2.1.1]hepta-2,5-diene)-molybdenum(0), $\text{Mo}(\text{CO})_4(\eta^{2,2}\text{-NBD})$ was prepared by refluxing a solution of hexacarbonylmolybdenum(0) and NBD in isooctane as described in literature.²⁵ The reaction solution was evaporated to dryness. Crystallization from n-hexane solution yields yellow crystals of the complexes. The solvent was decanted and crystals were dried in vacuum. IR (in toluene): $A_1^{(2)} = 2040$, $A_1^{(1)}$, $B_1 = 1951$, $B_2 = 1887 \text{ cm}^{-1}$.

3.10.2. Synthesis of the Mo(CO)₄(η^{2:2}-1,5-cyclooctadiene)

Tetracarbonyl(η^{2:2}-1,5-cyclooctadiene)molybdenum(0), Mo(CO)₄(η^{2:2}-COD) was prepared by refluxing Mo(CO)₆ and 1,5-cyclooctadiene (COD) in n-heptane as described in the literature.¹⁷ Solvent and excess COD were removed in vacuum and the residue was dissolved in n-hexane and filtered. Cooling the solution to -35 °C yielded yellow crystals of Mo(CO)₄(η^{2:2}-COD), which were dried in vacuum and identified by means of IR spectroscopy. IR (in toluene) A₁⁽²⁾ = 2036, A₁⁽¹⁾, B₁ = 1942, B₂ = 1880 cm⁻¹.

3.10.3. Synthesis of the N,N'-Bis(ferrocenylmethylene)ethylenediamine

Schiff-Base containing ferrocenyl groups can be obtained by the reaction of ferrocenyl amine with an appropriate aldehyde or with ferrocenylcarboxyaldehyde and appropriate amine.²⁶ The N,N'-Bis(ferrocenylmethylene)-ethylenediamine was prepared by using the procedure given in the literature:²⁷ Ferrocenecarboxaldehyde, which can also be synthesized by using the literature procedure²⁸, (2.180 g, 10.2 mmol) was dissolved completely in 30 cm³ of benzene at room temperature. Then 0.306 g (5.1 mmol) of ethylenediamine was added. The flask containing the reaction mixture was connected to a condenser equipped with a Dean-Stark apparatus and refluxed for 3 hours in a glycerine bath. After hot solution was filtered, it was dried in a rotary evaporator to obtain a yellow precipitate. Crystallization from 1:10 CH₂Cl₂ / n-hexane solution yielded yellow crystals of C₂₄H₂₄N₂Fe₂ (2.3 g, 98% yield), which were dried in vacuum. IR (CH₂Cl₂) ν(C=N) = 1646 cm⁻¹; UV-VIS (CH₂Cl₂) λ_{max} = 234 (CT), 267 (CT), 346 (d-d transition of iron centers), 460 nm (d-d transition of iron centers); ¹H-NMR (δ ppm, in CDCl₃): δ = 8.1(s, 2H, -CH=N-), 3.7 (s, 4H, -CH₂), 4.1 (s, 10H, C₅H₅), 4.3 (s, 4H, β-hydrogen of C₅H₄-) and 4.5 (s, 4H, α-hydrogen of C₅H₄-) ppm; ¹³C-NMR (δ ppm, in CDCl₃): δ = 162.661 (-C=N-), 62.6 (-CH₂), 69.7 (C₅H₅), 68.8 (β-Carbons of C₅H₄-), 70.7 (α-Carbons of C₅H₄-), 80.9 (ipso-Carbons of C₅H₄-); CV (CH₂Cl₂) Ox. Pot. = 0.567V, Red. Pot. = 0.462V.

3.10.4. Synthesis of the Tetracarbonyl[N,N'-bis(ferrocenylmethylene)ethylenediamine]molybdenum(0), Mo(CO)₄(BFEDA)

A quantity of 0.45 g (1.42 mmol) of Mo(CO)₄(η^{2:2}-NBD) was dissolved in 15 mL of toluene. Then, 0.58 g (1.28 mmol) of N,N'-Bis(ferrocenylmethylene)ethylene diamine (BFEDA) was added to the above solution with stirring at room temperature. The mixture was stirred for three days with a magnetic stirrer. The reaction was followed by monitoring the IR spectra of the samples taken from the reaction solution during the reaction. When the ligand exchange reaction was completed, the solution was brought to the dryness under vacuum. The solid residue was then washed with n-hexane in order to remove any Mo(CO)₄(η^{2:2}-NBD), NBD ligand itself, and other n-hexane soluble impurities. The yellow remnant was dissolved in 1:1 CH₂Cl₂/n-hexane solution for recrystallization. Yellow-orange, needle like crystals of Mo(CO)₄(BFEDA) were obtained after waiting for 5 days at -35 °C. The complex was also prepared starting with Mo(CO)₄(η^{2:2}-COD) and BFEDA following the same procedure. Yield: 68%. Anal. Found C, 49.5; H, 3.6; N, 4.2. C₂₈H₂₄Fe₂MoN₂O₄. Cal.: C, 51.0; H, 3.8; N, 4.2. IR ν(C=O) in CH₂Cl₂): A₁⁽²⁾ = 2011, B₁ = 1894, A₁⁽¹⁾ = 1875, B₂ = 1824 cm⁻¹; ν(C=N) = 1618 cm⁻¹. UV-VIS (CH₂Cl₂) λ_{max}: 236(CT), 259 (CT), 304(d-d transition of 4d electrons of Mo(0)), 348 (d-d transition of 3d electrons of Fe(II)), 480 nm (d-d transition of 3d electrons of Fe(II)); CV(CH₂Cl₂) Ox. Pot. = 0.46 V (Mo/Mo⁺), 0.59 V (Ferrocene/Ferrocenium⁺), 0.69 V (Ferrocene/Ferrocenium⁺), 0.83 V (Mo⁺/Mo⁺³) Red. Pot. = 0.58 V (Ferrocenium⁺/Ferrocene), 0.67 V (Ferrocenium⁺/Ferrocene), 0.79 V (Mo⁺³/Mo⁺); ¹H-NMR (δ ppm, in CD₂Cl₂): δ = 8.44 (s, 2H, -CH=N-), 3.8 (s, 4H, -CH₂), 4.2 (s, 10H, C₅H₅), 4.6 (t, J = 6 Hz, 4H, β-hydrogen of C₅H₄) and 5.1 (t, J = 2Hz, 4H, α-hydrogen of C₅H₄) ppm; ¹³C-NMR (δ ppm, in CD₂Cl₂): δ = 170.8 (-C=N-), 66.6 (-CH₂), 70.1 (C₅H₅), 72.6 (α-Carbons of C₅H₄-) and 72.3 (β-Carbons of C₅H₄-), 77.7 (ipso-carbons of C₅H₄-), 222.5 and 207.9 (CO) ppm; MS m/z = 662 (M⁺), 634 (M⁺-CO), 606 (M⁺-2CO), 578 (M⁺-3CO), 550 (M⁺-4CO).

CHAPTER 4

RESULTS AND DISCUSSION

4.1. N,N'-Bis(ferrocenylmethylene)ethylenediamine, BFEDA

The N,N'-Bis(ferrocenylmethylene)ethylenediamine, BFEDA, was synthesized according to the procedure given in the literature²⁷ from condensation reaction of ferrocenecarboxaldehyde and ethylenediamine. Firstly, ferrocenecarboxaldehyde was dissolved in benzene, and ethylenediamine was added to the solution. Reaction mixture was refluxed about three hours with a dean-stark apparatus to remove water-benzene azeotrope from refluxing solution since imine molecule hydrolyzes in the presence of water. The condensation reaction was followed by IR spectroscopy. As the absorption band at 1685 cm^{-1} for the CO stretching decreases, a new band at 1644 cm^{-1} , due to stretching of C=N bond, grows in. After reaction was ceased, solution was cooled and solvent was removed by rotary-evaporator.

The yellow crystals of BFEDA were characterized by using IR, Raman, UV-VIS and NMR spectroscopy techniques. The IR spectrum of the BFEDA taken in CH_2Cl_2 solution shows a characteristic sharp peak at 1644 cm^{-1} due to the stretching of $-\text{C}=\text{N}-$ group for which the stretching frequency is expected to be in the range of $1500\text{-}1680\text{ cm}^{-1}$ (Figure 4.1). The observation of this absorption band is a compelling evidence for the formation of the $-\text{C}=\text{N}-$ bond.

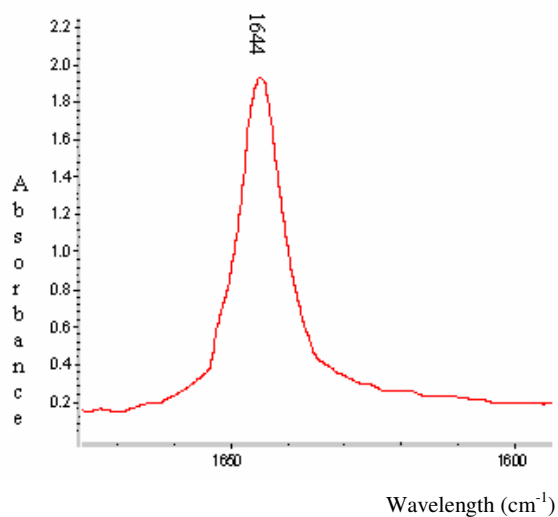


Figure 4.1. IR spectrum of the BFEDA in CH_2Cl_2

The two-imine bonds in the BFEDA molecule have a zigzag shape as shown in the Figure 4.2. Thus, there are two stretching modes; one is symmetric, the other is antisymmetric stretching. While one mode is Raman active, the other is IR active because for the molecules with a center of symmetry, it is not possible for a vibration to be active in both kinds of spectrum.²⁹ This statement was proved for the BFEDA and can be seen in Raman (1644 cm^{-1}) and IR (1640 cm^{-1}) spectrum taken from solid and KBr disc respectively (Figures 4.3 and 4.4.)

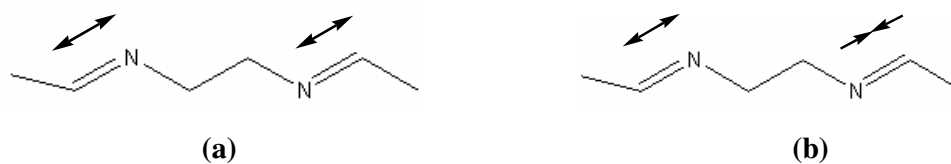


Figure 4.2. Representation of stretching modes in BFEDA
 (a) Symmetric stretching, (b) Antisymmetric stretching

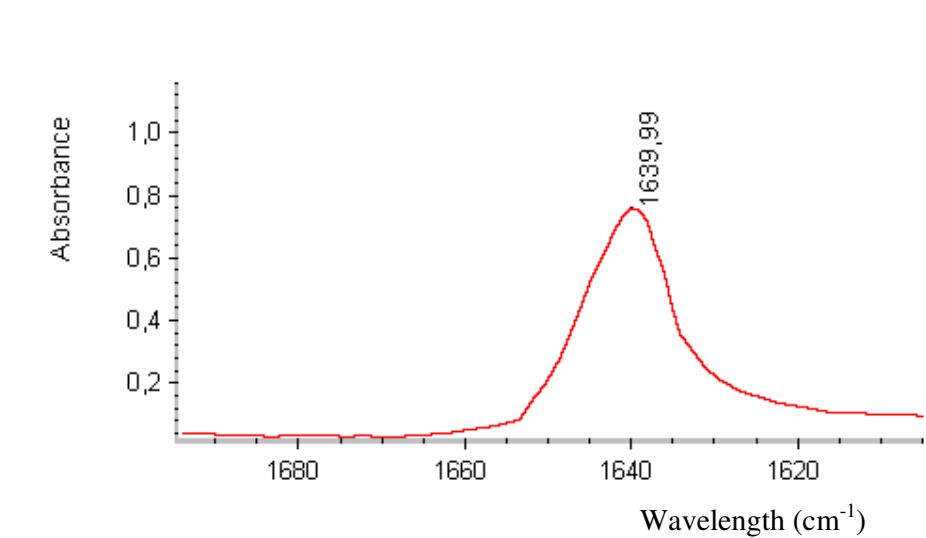


Figure 4.3. Infrared spectrum of BFEDA taken from KBr disc

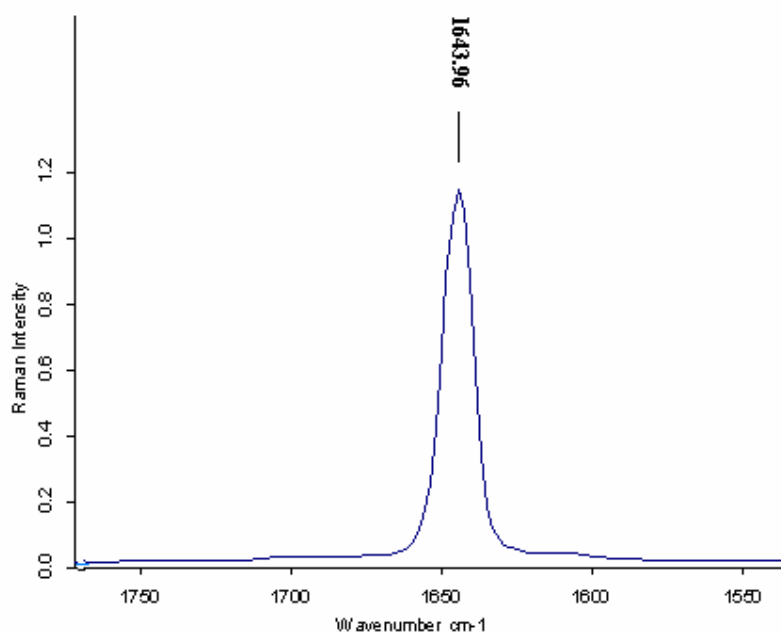


Figure 4.4. Raman spectrum of the BFEDA in solid form.

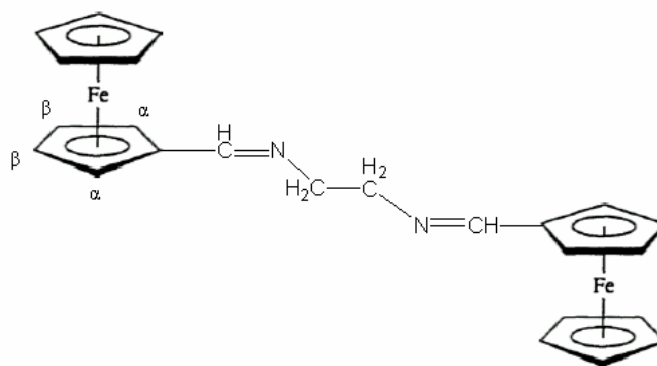


Figure 4.5. Suggested structural formula of BFEDA.

The $^1\text{H-NMR}$ spectrum of the BFEDA molecule is given in Figure 4.6. In ferrocenyl region of $^1\text{H-NMR}$ spectrum (4-5 ppm), three peaks are observed; a singlet at 4.1 ppm for the five equivalent hydrogen atoms of unsubstituted cyclopentadienyl ring and two singlets at 4.3 and 4.5 ppm for hydrogen of monosubstituted cyclopentadienyl ring. The hydrogen atoms of the methylene group give a signal at 3.7 ppm. The hydrogen atoms of imine bonds ($-\text{CH}=\text{N}-$) resonate at 8.1 ppm, a value comparable with the corresponding signal for analogous aliphatic imines.³⁰

Due to electron withdrawing effect of substituents, protons of substituted cyclopentadienyl ring are at lower field than protons of unsubstituted cyclopentadienyl ring.

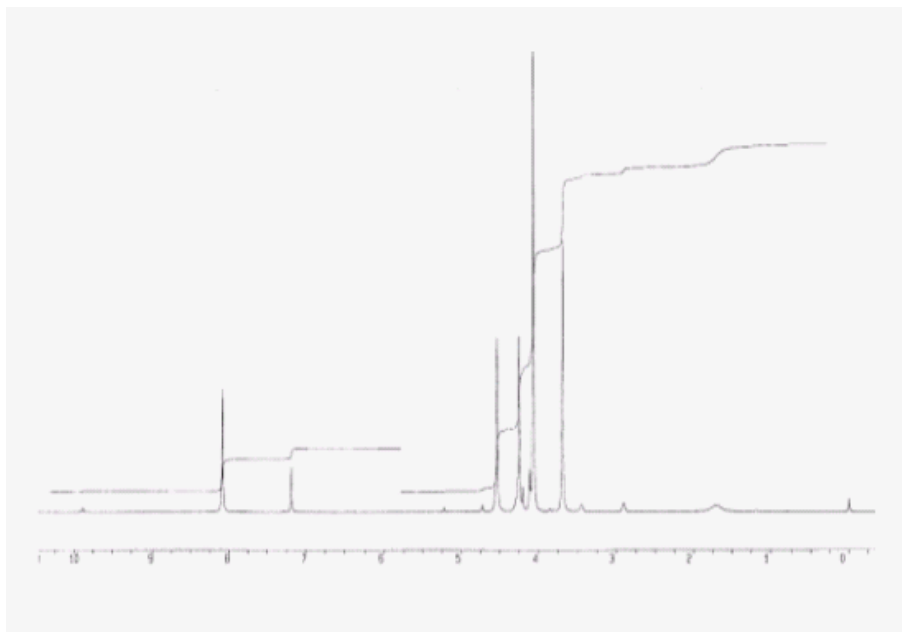
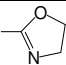
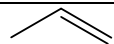
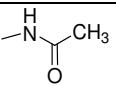
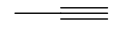
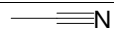
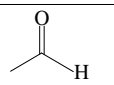
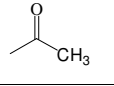
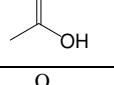
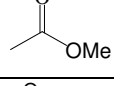
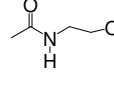
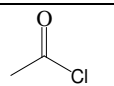
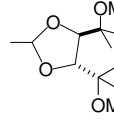


Figure 4.6. $^1\text{H-NMR}$ spectrum of BFEDA in CDCl_3

Table 4.1 lists the chemical shifts of the α -, β - and C_5H_5 - hydrogen atoms in twenty nine substituted ferrocene derivatives relative to ferrocene itself (4.19 ppm).³¹ The assignment of α and β positions of C_5H_4 in **1**, **4**, **6**, **8** and **9** have previously been achieved by comparison of their spectra. Also for category of electron-accepting substituted ferrocenes ($\delta_\alpha > \delta_\beta > 0$), peaks were assigned by NOE experiment, which was carried out between ortho-hydrogen of phenyl group and α position (3% enhancement) for the phenyl ferrocene molecule. The uniformity of sulfide-sulfoxide-sulfone series (**20-22**) is matched by that of halogens (**23-26**) in which α , β assignments ($\delta_\alpha > 0$, $\delta_\beta < 0$) have been established by deuterium labeling and on this basis the β positions of **18** are also assigned to upfield signal similarly, the amine and hydroxy substituents of **17** and **19** both results in an upfield shift with the effect on the β positions being greatest ($\delta_\beta < \delta_\alpha < 0$). Due to electropositive character, three of substituents (**14**, **28**, **29**) fell into a final category ($\delta_\alpha < 0$, $\delta_\beta > 0$). As a result, the signal at 4.5 ppm shown in $^1\text{H-NMR}$ spectrum of BFEDA was assigned to be α protons of C_5H_4 (substituted cyclopentadienyl ring) and the signal at 4.3 ppm was assigned to β protons of C_5H_4 . The last signal at 3.7 ppm seen in $^1\text{H-NMR}$ spectrum of the BFEDA belongs to resonance of methylene protons ($-\text{CH}_2-\text{CH}_2-$). In

addition, integration of protons from low field to high field is 1:2:2:5:2 which is the indication of presence of a two fold symmetry operation in the BFEDA molecule.

Table 4.1. Changes in chemical shifts for α , β and C_5H_5 positions relative to ferrocene (4.19 ppm). All spectra were recorded at room temperature in $CDCl_3$ on a 400 MHz instrument. 'b' denotes where the triplet peaks with $J = 1.45$ - 2.14 Hz, were resolved.

		α^b	β^b	C_5H_5			α^b	β^b	C_5H_5
1	-CH ₃	-0.11	-0.15	-0.08	15		0.56	0.15	0.01
2	-CH ₂ OH	0.00	0.03	0.00	16	-NO ₂	1.06	0.33	0.15
3	-CH ₂ NMe ₂	-0.04	-0.1	-0.1	17	-NH ₂	-0.17	-0.32	-0.07
4		0.03	0.17	-0.08	18		0.38	-0.19	-0.02
5	-Ph	0.46	0.13	-0.13	19	-OH	-0.20	-0.43	-0.05
6		0.28	0.02	0.04	20	-SPh	0.22	0.15	0.08
7		0.48	0.21	0.16	21	-SOPh	0.32	0.18	0.20
8		0.55	0.36	0.02	22	-SO ₂ Ph	0.50	0.22	0.31
9		0.59	0.32	0.02	23	-F	0.13	-0.39	0.09
10		0.68	0.28	0.07	24	-Cl	0.21	-0.13	0.06
11		0.61	0.20	0.01	25	-Br	0.23	-0.08	0.05
12		0.50	0.18	0.04	26	-I	0.23	-0.03	0.01
13		0.74	0.39	0.16	27	-TMS	-0.06	0.17	-0.03
14		-0.04	0.17	0.02	28	-SnBu ₃	-0.12	0.19	-0.04
					29	-PPh ₂	-0.12	0.14	-0.15

The ^{13}C -NMR spectrum of BFEDA (Figure 4.7) shows three signals at 80.9, 70.7 and 68.8 ppm for the carbons of the substituted cyclopentadienyl ring and one signal at 69.7 ppm for the carbons of the substituted cyclopentadienyl ring. The chemical shift of the carbons of the imine group is at 162.7 ppm and methylene carbon's is at 62.6 ppm.

The carbon of imine ($>\text{C}=\text{N}-$) gives a signal at a range of 165-145 ppm in ^{13}C -NMR spectrum. In ^{13}C -NMR spectrum of BEFDA, the signal at 162.6 ppm is assigned to carbon atom of imine group ($-\text{CH}=\text{N}-$). As the ipso carbon (carbon does not have attached hydrogen) of substituted cyclopentadienyl ring is the closest to the electron-withdrawing imine moiety, it is the most deshielded carbon in the ferrocene molecule. The chemical shift of ipso carbon is at 80.9 ppm and its low intensity is also an indication of a quaternary carbon. The five equivalent hydrogen of unsubstituted cyclopentadienyl ring gives a signal at 69.7 ppm and because of being far away from electron-withdrawing imine moiety, these carbon are the least deshielded carbon of the ferrocene, same as the protons of unsubstituted cyclopentadienyl ring observed in ^1H -NMR spectrum. The β carbons of substituted cyclopentadienyl ring resonate at 70.7 and 68.8 ppm, respectively.

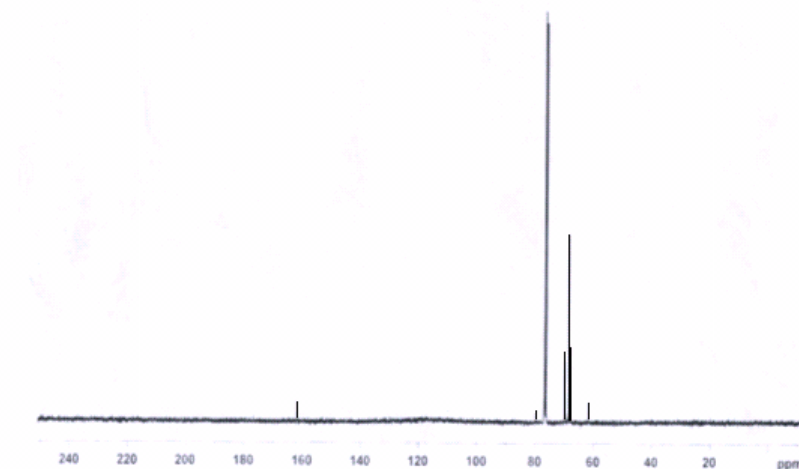


Figure 4.7. $^{13}\text{C}\{-^1\text{H}\}$ -NMR spectrum of the BFEDA in CDCl_3

The UV-VIS spectrum of the BFEDA given in Figure 4.8 shows four absorption bands at 234, 267, 346 and 460 nm.

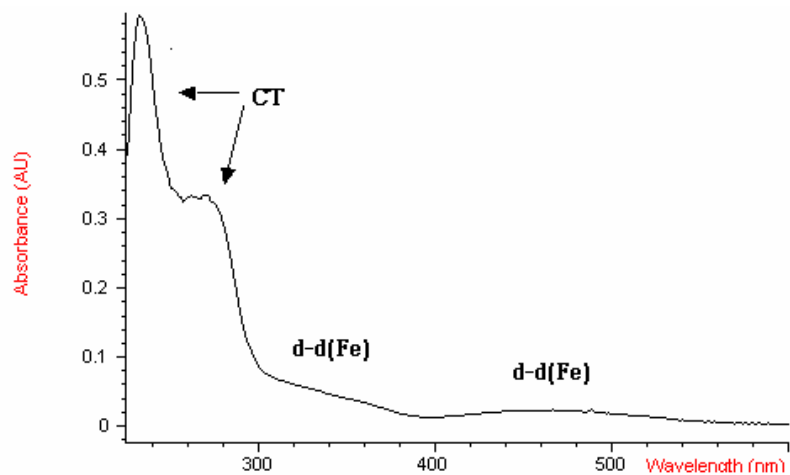


Figure 4.8. The UV-VIS spectrum of the BFEDA in CH_2Cl_2 , taken at room temperature.

The d^6 metallocenes exhibit two low-intensity bands in visible region. These have been assigned to be d-d transitions. Using strong-field theory, three spin-allowed d-d transitions are expected for free and substituted ferrocene.

The spin allowed ligand field absorption bands and charge transfer transitions of free ferrocene is given in Table 4.2. These bands are comparable with d-d transition of BFEDA molecule. Therefore the band at 346 and 460 nm in UV-VIS spectrum of the BFEDA are assigned to d-d transition of iron (II) center.

Table 4.2. The electronic absorption bands of free ferrocene.

Absorption wavelength (nm)	Extinction coefficient
458	9.1
324	49
265	1600
239	3500
200	51000

The free ferrocene has three charge transfer transitions as have been reported in the literature (i.e. 200, 239, 265 nm).³² The higher energy charge transfer has been reported to be MLCT transition. Characterizations of other two charge transfer transitions have not been defined. Therefore, in the UV-VIS spectrum of the BFEDA molecule, the bands at 234 nm and 267 nm are assigned to be charge transfer transition.

4.2. Tetracarbonyl[N,N'-bis(ferrocenylmethylene)ethylenediamine]molybdenum(0)

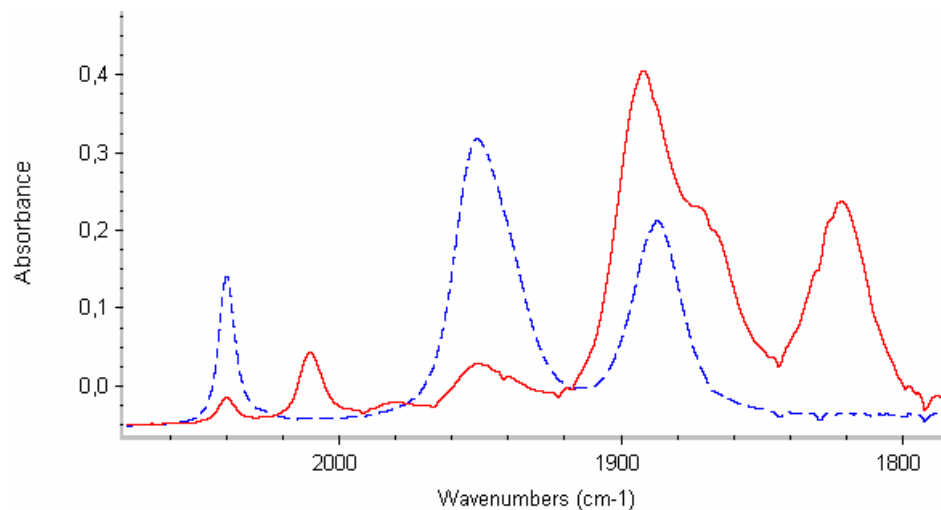
The substitution reaction between N,N'-bis(ferrocenylmethylene)ethylenediamine (BFEDA) and $\text{Mo}(\text{CO})_4(\eta^{2:2}\text{-NBD})$ in toluene yields the tetracarbonyl[N,N'-bis(ferrocenylmethylene)ethylenediamine]molybdenum(0). Since heating causes to the decomposition of $\text{Mo}(\text{CO})_4(\eta^{2:2}\text{-NBD})$ to $\text{Mo}(\text{CO})_6$, the reaction solution was stirred at room temperature. The substitution reaction of NBD by BFEDA was completed in three days at room temperature as followed by IR spectroscopy. At the beginning of the reaction IR spectrum shows three absorption bands at 2040, 1951 and 1887 cm^{-1} of the starting complex. The $\text{Mo}(\text{CO})_4(\eta^{2:2}\text{-NBD})$ has a local C_{2v} symmetry for $\text{Mo}(\text{CO})_4$ moiety so four $\nu(\text{CO})$ vibrations are expected; $2A_1$, B_1 , B_2 , all of them being IR active absorption.³³ Since only three absorption bands were observed, the two of four bands (B_1 , $A_1^{(1)}$) are coincidentally overlapping. During the reaction, the three bands of $\text{Mo}(\text{CO})_4(\eta^{2:2}\text{-NBD})$ disappeared gradually and four new bands grow in concomitantly (Figure 4.9. a) along with a feature at 1982 cm^{-1} due to $\text{Mo}(\text{CO})_6$. Upon evaporation of solvent under vacuum yellow solid was obtained. Then, the residue was washed 10 times with n-hexane to remove NBD. Crystallization from the solution of 1:1 $\text{CH}_2\text{Cl}_2/\text{n-hexane}$ at a temperature of $-35\text{ }^\circ\text{C}$ yielded the tetracarbonyl[N,N'-bis(ferrocenylmethylene)ethylenediamine]molybdenum(0) complex in orange crystals (yield 68 %). The thermal substitution of $\text{Mo}(\text{CO})_4(\eta^{2:2}\text{-COD})$ with BFEDA gave the same product which was isolated by following the same procedure. Thus, both $\text{Mo}(\text{CO})_4(\eta^{2:2}\text{-NBD})$ and $\text{Mo}(\text{CO})_4(\eta^{2:2}\text{-COD})$ can be used as $\text{Mo}(\text{CO})_4$ transfer reagents for the synthesis of

Mo(CO)₄(BFEDA). The difference in the dissociation energy of metal-olefin bond (M-ll) in two complexes is just 2 kcal/mol,³⁴ and COD requires larger coordination site than NBD.¹⁰

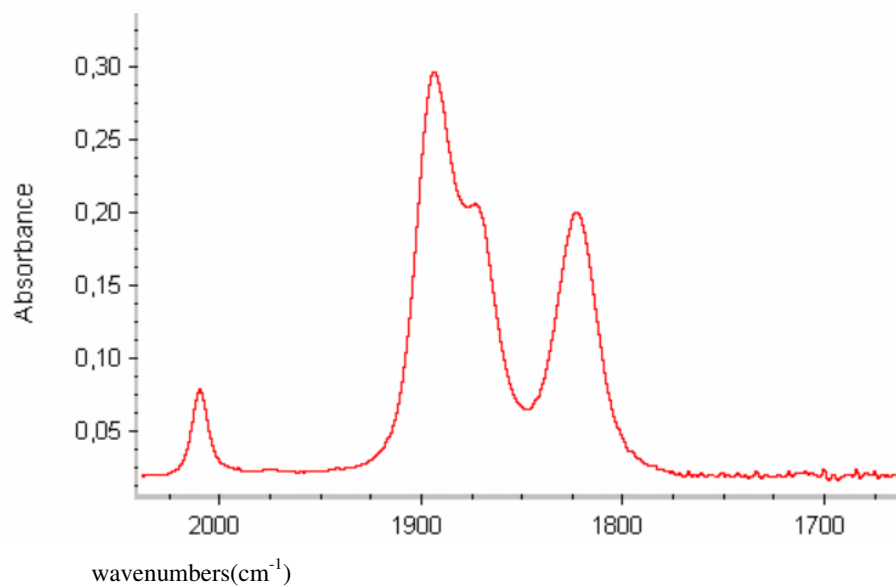
The complex Mo(CO)₄(BFEDA) was characterized by means of elemental analysis, IR, ¹H-, ¹³C-¹H-NMR, UV-VIS and mass spectroscopy methods. The IR spectrum of Mo(CO)₄(BFEDA) is given in Figure 4.9.b. The observation of four absorption bands at 2011, 1894, 1875 and 1824 cm⁻¹ for the CO stretching indicates that the Mo(CO)₄(BFEDA) complex has a local symmetry of C_{2v}, which gives four IR active vibration modes of 2A₁, B₁ and B₂ for the CO stretching.

The CO stretching frequencies for the three molybdenumtetracarbonyl complexes are listed in Table 4.3. It can be seen that, the CO stretching frequencies of Mo(CO)₄(BFEDA) are lower compared to the respective bands of Mo(CO)₄(η^{2:2}-NBD) and Mo(CO)₄(η^{2:2}-COD). This indicates a lower extend of π-accepting ability of BFEDA than the olefins, because C-O stretching frequencies of metal carbonyls decreases as extend of the π-electron donation from metal to carbonyl group increased.³⁵

The C=N stretching frequency of the imine bond shifts from 1644 cm⁻¹ for the free BFEDA molecule to 1618 cm⁻¹ in the Mo(CO)₄(BFEDA). This decrease in the C=N stretching frequency upon coordination is in agreement with previous studies.³⁶ This indicates a weakening of C=N bond upon coordination to the Mo(CO)₄ fragment. Thus, the change in stretching frequency shows that the BFEDA coordinates to the metal through the two nitrogen atoms.



(a)



(b)

Figure 4.9. (a) IR spectrum of the solution taken in toluene during the reaction of $\text{Mo}(\text{CO})_4(\eta^{2:2}\text{NBD})$ with BFEDA; the dashed line denotes the spectrum of $\text{Mo}(\text{CO})_4(\eta^{2:2}\text{NBD})$ complex and solid line the spectrum of $\text{Mo}(\text{CO})_4(\text{BFEDA})$, (b) IR spectrum of the $\text{Mo}(\text{CO})_4(\text{BFEDA})$ complex in toluene after purification.

Table 4.3. The CO stretching frequencies of complexes having Mo(CO)₄ moiety (in cm⁻¹) as observed in the IR spectra taken from toluene solution.

Compound	A ₁ ⁽²⁾	B ₁	A ₁ ⁽¹⁾	B ₂
Mo(CO) ₄ (η ^{2:2} -NBD)	2040	1951		1887
Mo(CO) ₄ (η ^{2:2} -COD)	2036	1942		1880
Mo(CO) ₄ (BFEDA)	2011	1894	1875	1824

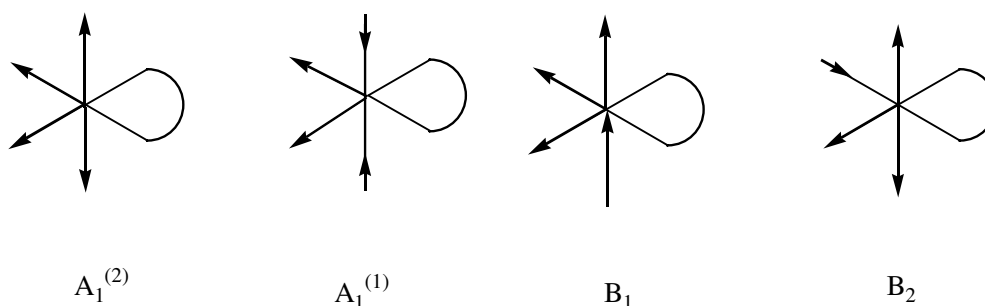


Figure 4.10. Symmetry coordinates for the CO stretching vibration modes in the cis-M(CO)₄L₂.

Infrared intensities of CO stretching vibrations in substituted metal carbonyl derivatives, M(CO)_mL_n have been shown to be highly dependent on the extend of M-CO π-bonding. The vibrations of the carbonyl bonds that are IR active are shown in Figure 4.10.

The intensity of A₁⁽²⁾ is a good indication of availability of π-electron density in metal-ligand bond. The vibronic contribution from π-bonding ligands is slightly enhancing the intensity of the A₁⁽²⁾ vibration.³⁷ The comparison of A₁⁽²⁾ intensity of Mo(CO)₄(η^{2:2}-NBD) and Mo(CO)₄(BFEDA) shows that A₁⁽²⁾ intensity is lower in latter complex. This proves the lower extend of π-accepting ability of BFEDA than this olefin.

The ¹H-NMR spectrum of Mo(CO)₄(BFEDA) shows similar pattern to that of the free BFEDA molecule. However, all peaks are shifted to lower magnetic field

upon coordination due to electron-withdrawing effect of Mo(CO)₄ moiety.

In ¹H-NMR spectrum, two singlets are seen at 5.1 and 4.6 ppm for the substituted cyclopentadienyl ring. Due to five equivalent hydrogen atoms of unsubstituted cyclopentadienyl ring, a singlet at 4.2 ppm is observed. The other two signals at 8.4 and 3.8 ppm correspond to the hydrogen atoms of imine and methylene group, respectively.

In ¹H-NMR spectrum of the complex Mo(CO)₄(BFEDA), the chemical shift of hydrogen attached to carbon of imine group is 8.4 ppm, compared to the value of 8.1 ppm for the free BFEDA molecule (Figure 4.11), one can see that, upon coordination the imine proton is more deshielded than free BFEDA molecule. The chemical shift of methylene proton (–CH₂–CH₂–) is 3.8 ppm, which is deshielded by 0.1 ppm with respect to free BFEDA molecule. In ferrocenyl region of spectrum, the least deshielded proton is again the five-equivalent-proton of unsubstituted cyclopentadienyl ring, whose chemical shift is 4.2 ppm. The change in chemical shift due to coordination is small for these hydrogen atoms. The resonances at 5.1 and 4.6 ppm are assigned to be α and β protons of substituted cyclopentadienyl ring. These two bands are seen as triplets, but it must be denoted as pseudo triplets because presence of different vicinal coupling constants there must be AA'BB' system for mono-substituted C_p rings in Mo(CO)₄(BFEDA) complex. The coupling constant between the α and β hydrogen atoms of the substituted cyclopentadienyl ring is 2 Hz.

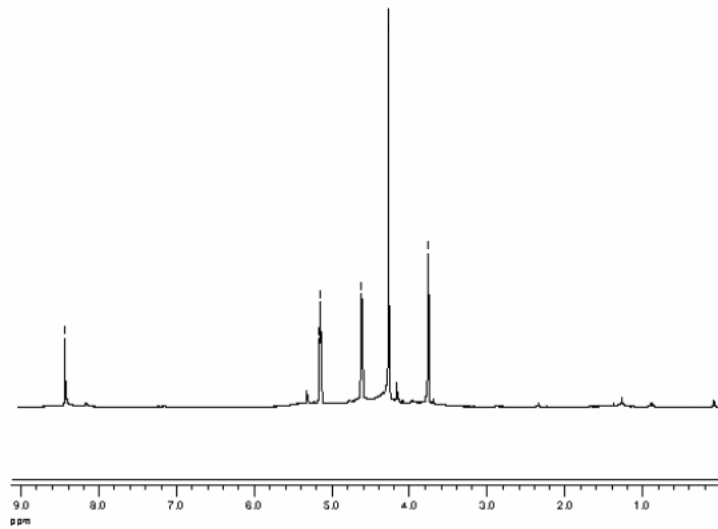


Figure 4.11. $^1\text{H-NMR}$ spectrum of $\text{Mo}(\text{CO})_4(\text{BFEDA})$ in CD_2Cl_2

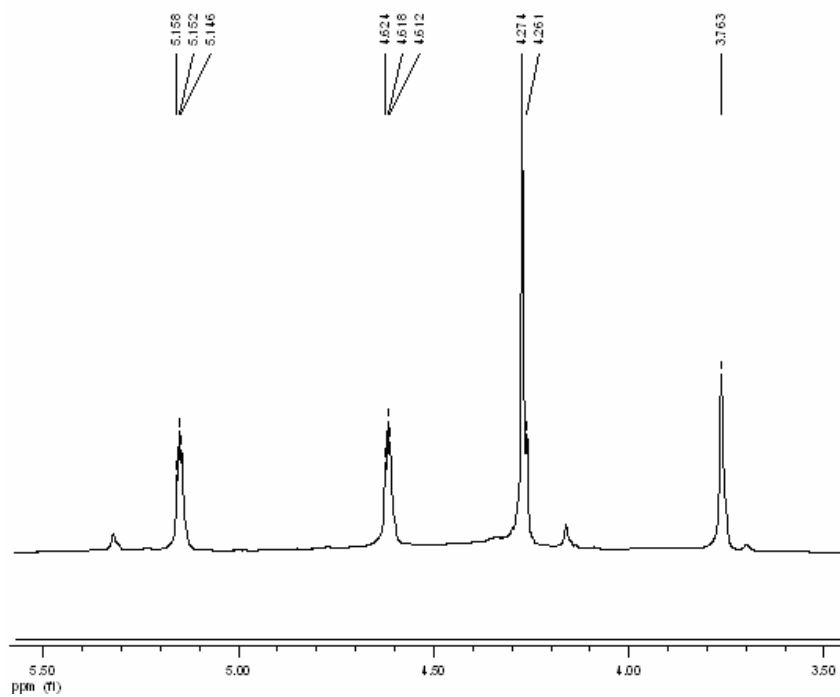


Figure 4.12. The $^1\text{H-NMR}$ spectrum of $\text{Mo}(\text{CO})_4(\text{BFEDA})$ in CD_2Cl_2 , the 5.50-3.50 ppm region expanded.

The ^{13}C - $\{^1\text{H}\}$ -NMR spectrum of the $\text{Mo}(\text{CO})_4(\text{BFEDA})$ was taken in CD_2Cl_2 (Figure 4.13). Except the ipso carbon of substituted cyclopentadienyl ring, all carbon chemical shifts are in a lower field than the corresponding carbons of free BFEDA molecule. The ^{13}C -NMR spectrum of $\text{Mo}(\text{CO})_4(\text{BFEDA})$ shows three singlets at 77.7, 72.6 and 72.3 ppm for substituted cyclopentadienyl ring and one signal at 70.1 ppm for unsubstituted cyclopentadienyl ring. The signals at 170.8 and 66.6 ppm correspond to carbon atoms of imine and methylene groups of BFEDA ligands.

The carbons of imine groups give signal at 170.8 ppm, which is deshielded by 8.2 ppm upon coordination to the $\text{Mo}(\text{CO})_4$ moiety. In ferrocenyl region of ^{13}C -NMR spectrum four signals appear. The signal at 70.1 ppm is for the carbons of unsubstituted cyclopentadienyl ring. These carbons are the least deshielded carbons compared with α and β carbons of substituted cyclopentadienyl ring whose chemical shifts are 72.6 and 72.3 ppm respectively. The ipso carbons resonate at 77.7 which 2.2 ppm higher chemical shift than the corresponding carbons in free BFEDA. Moreover, the methylene carbons give signal at 66.6 ppm.

The shielding of the ipso carbons can be interpreted by delocalization of electrons via conjugation. In addition, the closeness for chemical shifts of α and β carbons (72.6 and 72.3 ppm, respectively) is also the result of delocalization of electrons. Thus, it can be concluded that, the BFEDA is a σ -donor ligand rather than a π -accepting ligand. As a result of the σ -donation of electrons from BFEDA to the Mo metal, α and β carbons are deshielded whereas ipso carbons are shielded upon coordination.

In addition to carbons of BFEDA ligand, there are four carbonyl carbons, which are pair wise equivalent and give two signals in ^{13}C -NMR spectrum at 207.9 and 222.5 ppm. The observation of two signals show a cis arrangement of four CO groups in the $\text{Mo}(\text{CO})_4$ moiety and also support the C_{2v} symmetry of complex.

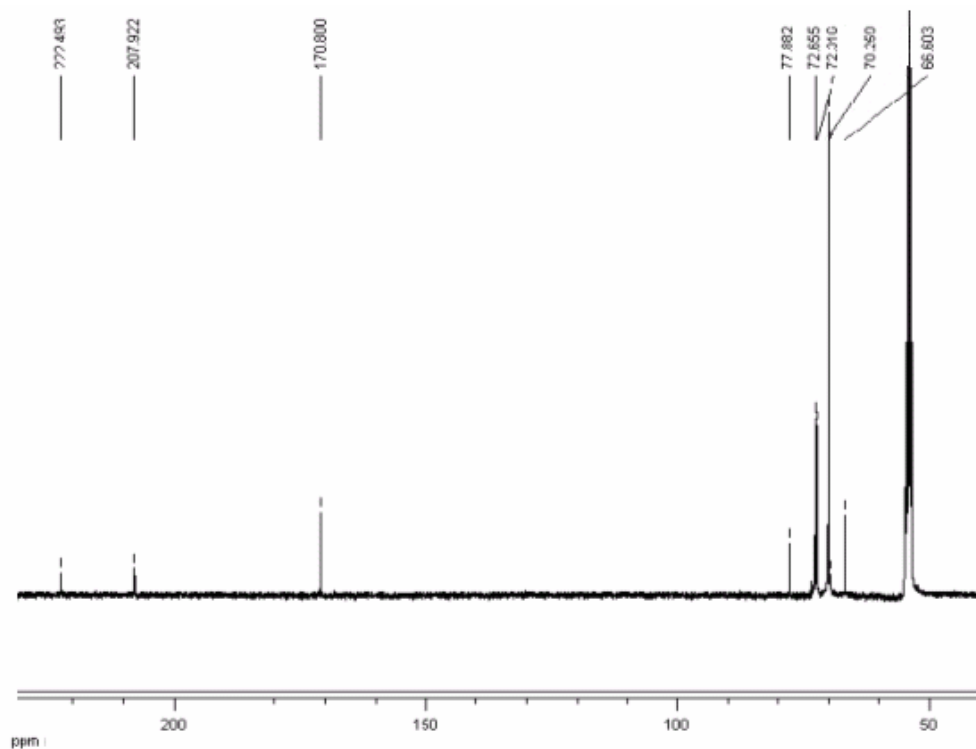


Figure 4.13. ^{13}C - $\{^1\text{H}\}$ -NMR spectrum of the $\text{Mo}(\text{CO})_4(\text{BFEDA})$ in CD_2Cl_2 .

The ^{13}C -NMR chemical shifts of the carbonyl ligands in three complexes with different ligands are listed in Table 4.4 for comparison. The comparison of the carbon chemical shifts shows that as the σ -donor ability of auxiliary ligands in $\text{M}(\text{CO})_4\text{L}_2$ complexes increases, the carbon atoms trans to σ -donor ligands are more deshielded (Table 4.5).

As the L group becomes a stronger σ donor or a poorer π acceptor ligand, the $\delta(^{13}\text{C})$ values are shifted to lower field. Moreover, since the $\delta(^{13}\text{CO}_{\text{cis}})$ value for a given complex is less than the $\delta(^{13}\text{CO}_{\text{trans}})$ value, the carbon atoms of the cis CO's are expected to be more susceptible to nucleophilic attack than are the carbon atoms of the trans CO.³⁸

Table 4.4. CO stretching frequencies and ^{13}C -NMR chemical shifts (δ , ppm) of the carbonyl groups of $\text{Mo}(\text{CO})_4(\text{L})_2$ complexes with three different ligands.^{17, 39}

	$\nu(\text{CO})$ (cm^{-1})	$\delta(\text{CO})_{\text{cis}}$	$\delta(\text{CO})_{\text{trans}}$
$\text{Mo}(\text{CO})_4(\text{COD})$	2034, 1939, 1889	216	216
$\text{cis-}[\text{Mo}(\text{CO})_4(\text{PPh}_2\text{H})_2]$	2026, 1926, 1914, 1892	215	209
$\text{Mo}(\text{CO})_4(\text{BFEDA})$	2011, 1894, 1875, 1824	207	222

For pentacarbonyl molybdenum complexes and tetracarbonyl chromium and tungsten complexes, the carbons in lower field in ^{13}C -NMR have been assigned to be trans to L ligand (Table 4.5 and 4.6). Therefore the chemical shift of 222 ppm in $\text{Mo}(\text{CO})_4(\text{BFEDA})$ is assigned to be trans to the BFEDA ligand, whereas the signal at 207 ppm is assigned to the CO groups cis to the BFEDA ligand.

Table 4.5. ^{13}C -NMR chemical shifts (δ , ppm) belonging to carbonyl groups of $\text{M}(\text{CO})_4(\text{L})_2$.⁴⁰

	$\delta(\text{CO})_{\text{cis}}$	$\delta(\text{CO})_{\text{trans}}$
$\text{cis-}[\text{H}_3\text{P}]_2\text{Cr}(\text{CO})_4$	218.4	224
$\text{cis-}[\text{Et}_3\text{P}]_2\text{W}(\text{CO})_4$	204.4	204.7

Table 4.6. ^{13}C -NMR chemical shifts (δ , ppm) belonging to carbonyl groups of $\text{Mo}(\text{CO})_5\text{L}$.⁴¹

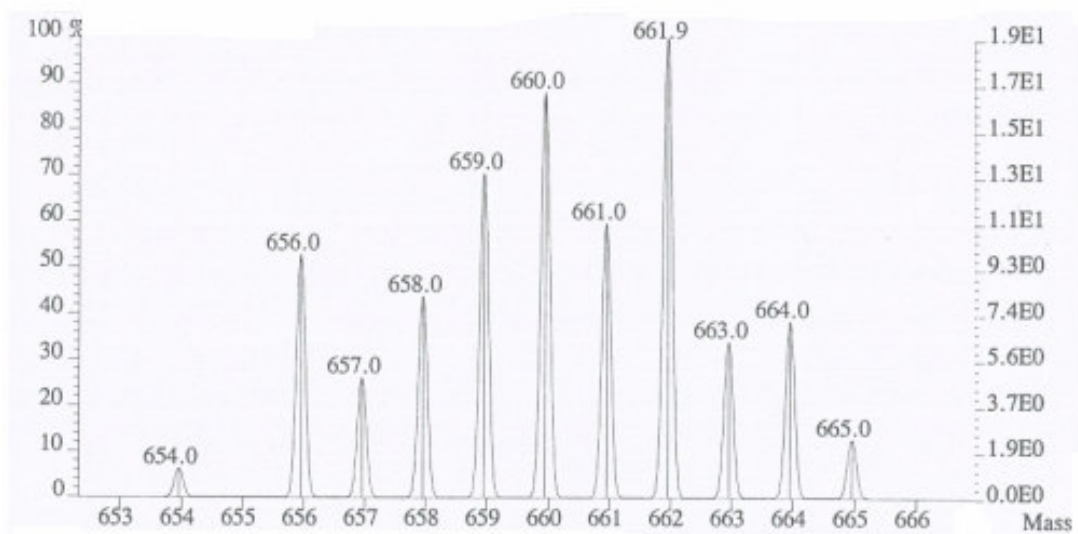
L	CO_{cis}	CO_{trans}
$\text{P}(\text{n-Bu})_3$	206.3	209.7
NMe_3	203.7	213.8
Py	204.2	214.3
$\text{P}(\text{OEt})_3$	204.7	208.6
$\text{P}(\text{Ome})_3$	204.3	208.2

Table 4.7 shows the elemental analysis results in the molecule, $C_{28}H_{24}Fe_2MoN_2O_4$. The experimental values are in agreement with the calculated values.

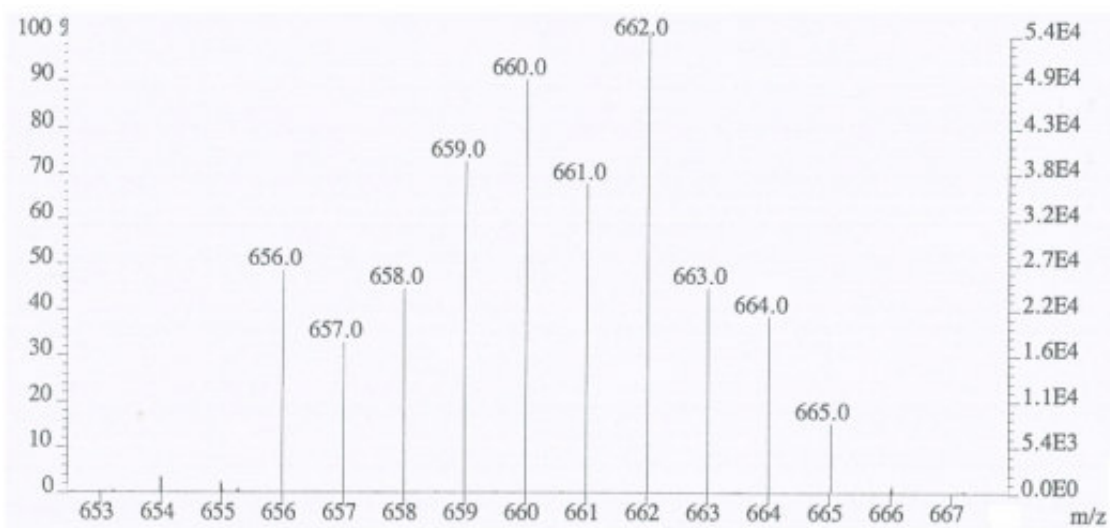
Table 4.7. The result of Elemental analysis for the complex $Mo(CO)_4(BFEDA)$

Atom	Found	Calculated for $C_{28}H_{24}Fe_2MoN_2O_4$
Carbon	49.5	51.0
Nitrogen	4.2	4.2
Hydrogen	3.6	3.8

Fast atom bombardment mass spectroscopy (FAB) was used further to characterize the $Mo(CO)_4(BFEDA)$ complex. The molecular peak with unique isotope distribution of $Mo(CO)_4(BFEDA)$ in mass spectrum is observed at $m/z= 662$ and perfectly fits to simulated molecular peak (Figure 4.14. a and b).



(a)



(b)

Figure 4.14. Molecular peaks of $\text{Mo}(\text{CO})_4(\text{BFEDA})$ in mass spectrum; **(a)** observed **(b)** simulated

The full mass spectrum of the $\text{Mo}(\text{CO})_4(\text{BFEDA})$ given in Figure 4.15 shows sequential detachment of four CO groups yielding fragments at $m/z = 634 (M^+ - \text{CO})$, $606 (M^+ - 2\text{CO})$, $578 (M^+ - 3\text{CO})$, $550 (M^+ - 4\text{CO})$]

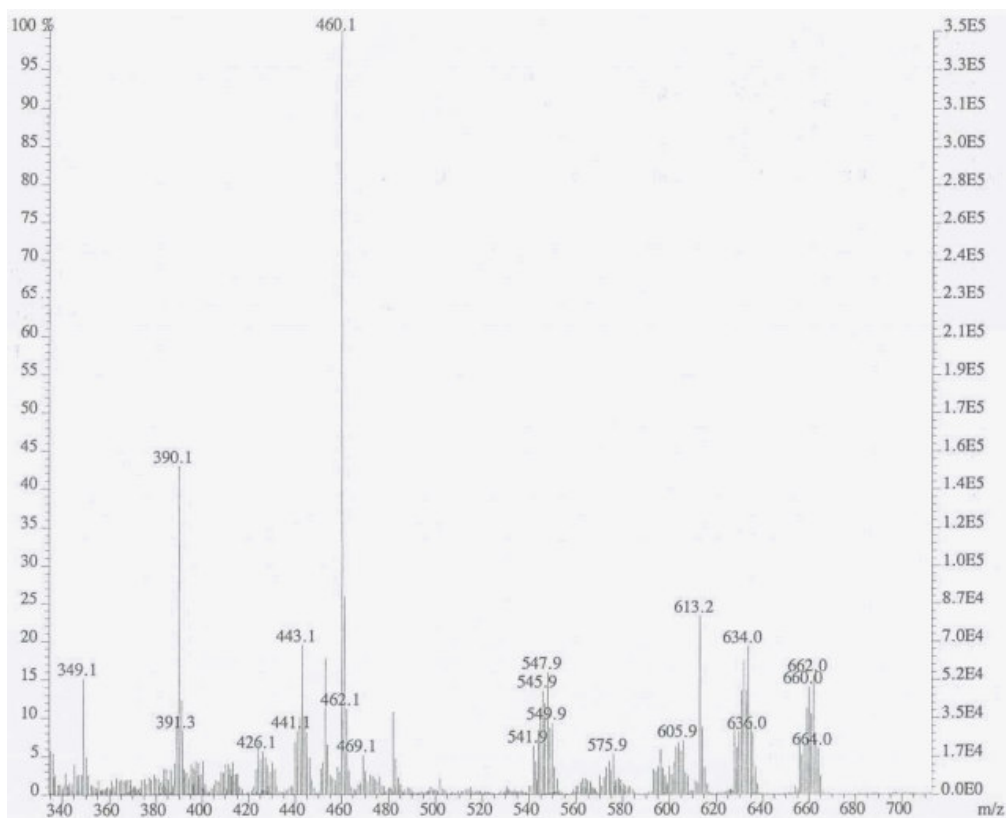


Figure 4.15. Mass spectrum of Mo(CO)₄(BFEDA).

In the UV-VIS spectrum of Mo(CO)₄(BFEDA) (Figure 4.16) the bands at 236 and 259 nm are assigned to charge transfer transitions of ferrocenyl moiety. The band at 304 nm is assigned to be d-d transition of Mo(0) (d⁶ ion) by comparing with reported spectra of various complexes.⁴² In addition, in the visible region, there are two absorption bands at 348 and 480 nm which are assigned to the d-d transition of Fe(II) and, therefore, having low intensity and not being dependent on solvent medium. Moreover, they are also present in the spectrum of free BFEDA molecule, these transitions are assigned to be d-d transitions of Fe(II).

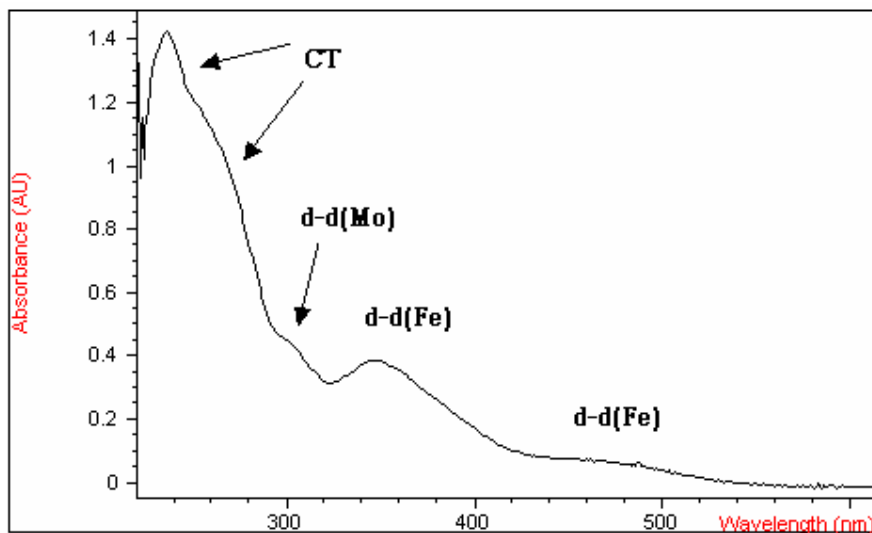


Figure 4.16. UV-VIS spectrum of $\text{Mo}(\text{CO})_4(\text{BFEDA})$ in CH_2Cl_2 taken at room temperature.

4.3. Electrochemistry of BFEDA and $\text{Mo}(\text{CO})_4(\text{BFEDA})$

Before studying the electrochemical behavior of the complex, $\text{Mo}(\text{CO})_4(\text{BFEDA})$, the electrochemical behavior of the free BFEDA molecule was investigated by recording the cyclic voltammogram, CV in CH_2Cl_2 . The cyclic voltammogram of the BFEDA exhibits one reversible oxidation at + 0.567 V (Figure 4.17). For a single, reversible, electron transfer, the half of the difference in cathodic and anodic peak potentials must be around 55-60 mV.²¹ The half of the difference between oxidation (0.567 V) and reduction peak (0.462 V) potentials is found to be 52 mV indicating a reversible one-electron transfer reaction. Furthermore, the ratio of cathodic peak current to anodic peak current, I_a/I_c , is almost unity at all scan rates which is a further evidence for the reversibility of electron transfer reaction.

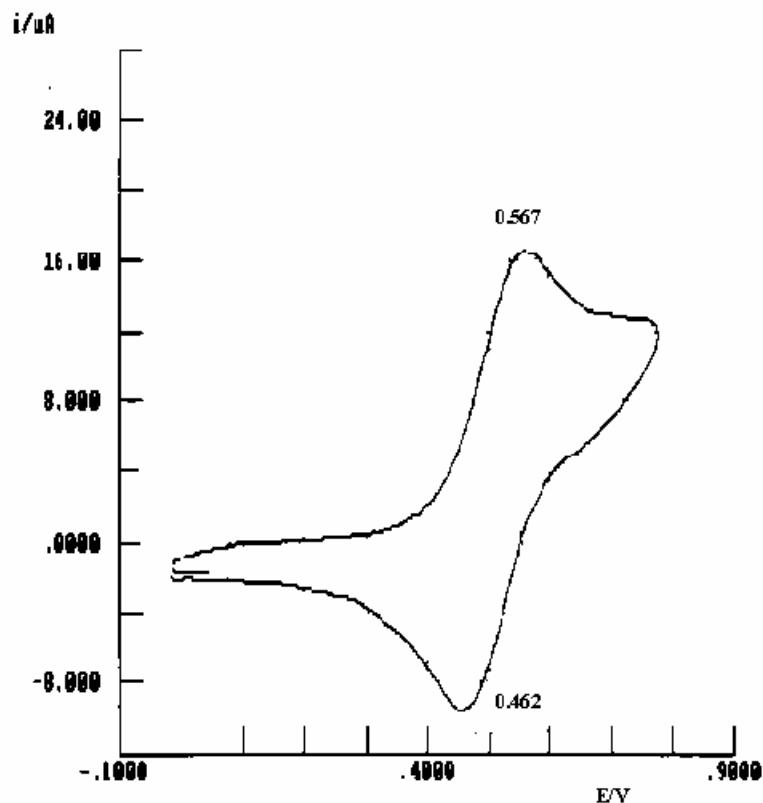


Figure 4.17. CV of BFEDA in CH_2Cl_2 solution containing TBABF_4 as supporting electrolyte. Voltage scan rate = 50 mV/s. Ag-wire is used as reference electrode.

Controlled potential electrolysis at the experimentally found oxidation potential (0.567 V) showed that oxidation was completed after the passage of 2 F. In the light of these findings, BFEDA can be considered as a molecule consisting of two equal non-interacting mono-electron redox groups that oxidize at the same potential.

Electrochemical behavior of the complex $\text{Mo}(\text{CO})_4(\text{BFEDA})$ was also investigated by recording the CV and differential pulse voltammetry in the same solvent-electrolyte couple at a voltage scan rate of 50 mV/s (Figure 4.18 and 4.19). During the anodic scan four oxidation peaks were observed at 0.46 V, 0.59 V, 0.69 V and 0.83 V. Based on the comparison with the free BFEDA molecule and their

reversibility, the second and third oxidation peaks at 0.59 and 0.69 V are assigned to the oxidation of ferrocene moieties. The two ferrocene moieties are no longer independent of each other; rather, they are electronically coupled by connection via the central molybdenum atom, leading to two distinct reversible oxidation processes, which are not fully resolved. The first (0.46 V) and fourth (0.83 V) oxidation peaks, not observable in the cyclic voltammogram of the free BFEDA molecule, are attributed to oxidation of molybdenum center based on the comparison with the cyclic voltammogram of a similar complex $\text{Mo}(\text{CO})_4(\text{bipy})$ (irreversible oxidation potentials; 0.52, 1.08 V with respect to saturated calomel electrode).⁴³

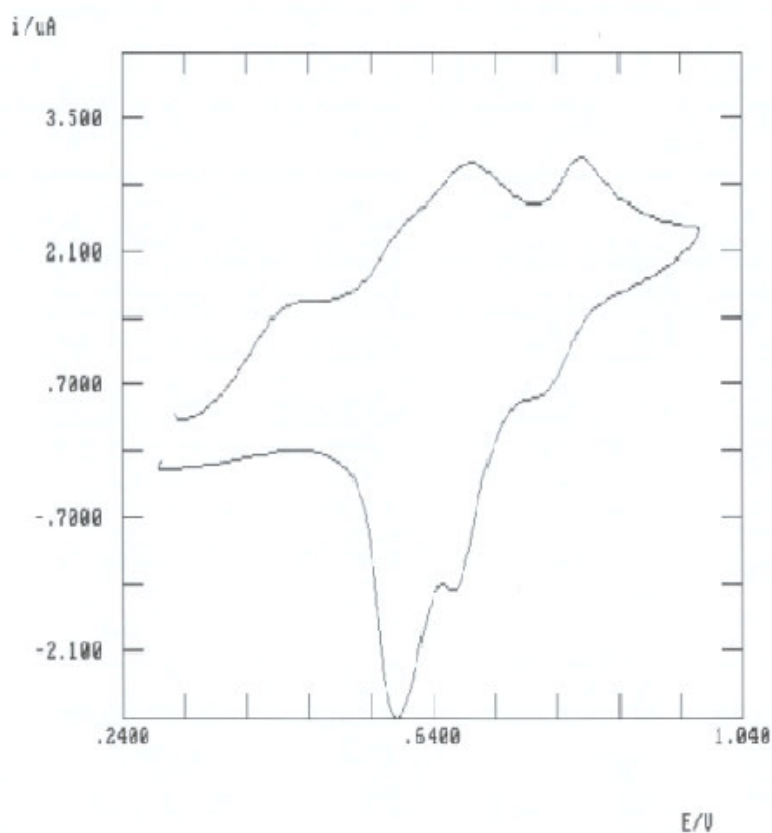


Figure 4.18. CV of 1×10^{-4} M solution of $\text{Mo}(\text{CO})_4(\text{BFEDA})$ in CH_2Cl_2 containing tetrabutylammonium tetrafluoroborate (0.1 M), with Ag-wire as reference electrode at a scan rate 50 mV/s.

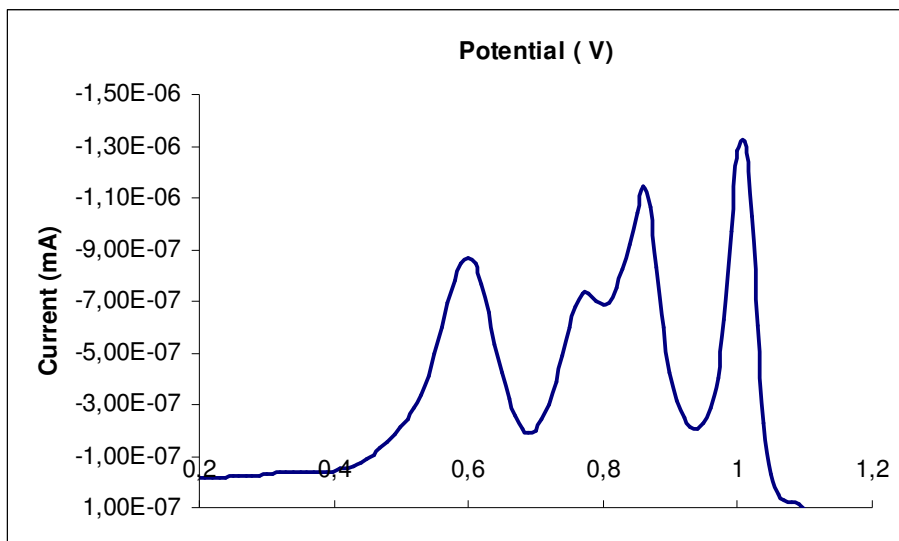


Figure 4.19. Differential pulse voltammogram of $\text{Mo}(\text{CO})_4(\text{BFEDA})$ (1×10^{-4} M) at a scan rate 50 mV/s in CH_2Cl_2 solution of tetrabutylammonium tetrafluoroborate (0.1 M) referenced to saturated calomel electrode(SCE).

The first oxidation peak at 0.46 V is an irreversible oxidation of Mo(0) to Mo(I). This type of irreversible oxidations of Mo(0) to Mo(I) and W(0) to W(I) have been reported in literature whereas oxidation of Cr(0) to Cr(I) has been reported to be reversible.⁴⁴ The poor chemical stability of oxidation products of molybdenum and tungsten complexes at room temperature may be responsible for irreversible oxidation of metal centers.

It is also found that the oxidation potential of ferrocene moieties in $\text{Mo}(\text{CO})_4(\text{BFEDA})$ are shifted towards more positive potential values by about 20-100 mV compared to free BFEDA. This shift is readily attributed to the electron withdrawing property of $\text{Mo}(\text{CO})_4$ that makes iron centers slightly more difficult to oxidize than that of free BFEDA molecule. During the reverse scan, three reduction peaks were observed at 0.58V, 0.67 V and 0.79 V. These reduction peaks are found to be related to oxidation processes that take place at 0.59 V, 0.69 V, and 0.83 V, respectively. As control the CV of the $\text{Mo}(\text{CO})_4(\text{BFEDA})$ was also taken by using

standard calomel electrode (SCE) as reference and is given in Figure 4.20 together with the CV recorded using Ag-wire as reference electrode. It is noteworthy that the CV with SCE exhibits the same number of oxidation and reduction peaks as in the CV with Ag-wire electrode, however, slightly shifted to higher potentials.

Bildstein and his coworkers have reported electrochemical study of similar group 6 metal carbonyl complexes with a bidentate ligand containing two ferrocenyl moieties, N,N'-diferrocenyldiazabutadiene (Fc-DAB).⁴⁵ They have found that the separation between two ferrocenyl oxidation peaks is 140 mV for Mo(CO)₄(Fc-DAB) and the separation increases in the order of Cr<Mo<W. In Mo(CO)₄(BFEDA) the separation of two oxidation is about 100 mV. This difference between two molybdenum complexes with two different diimine ligands can be attributed to degree of conjugation between two ferrocenyl moieties in these compounds.

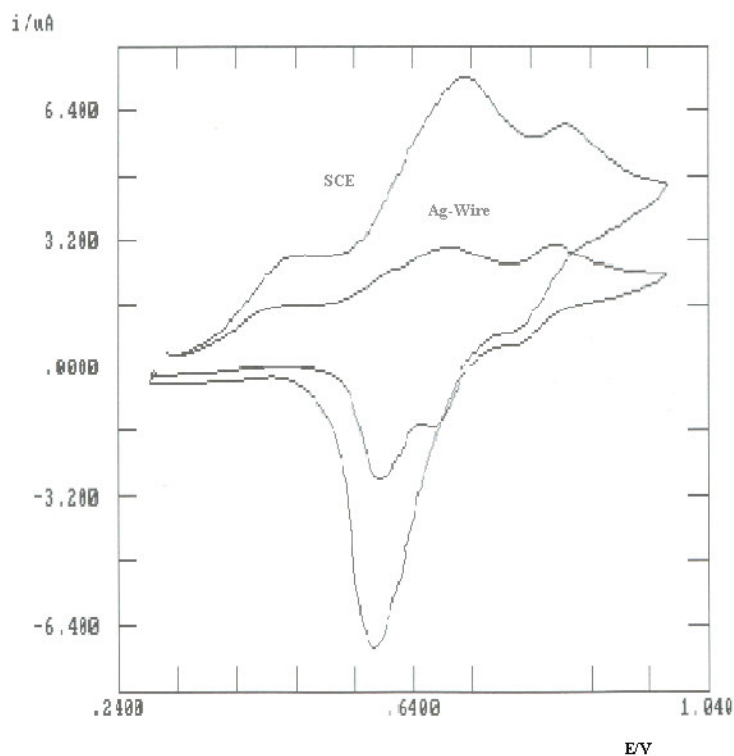


Figure 4.20. CV of Mo(CO)₄(BFEDA) at a scan rate 50 mV/s with reference electrode of Ag-wire and SCE.

The effect of voltage scan rate on the oxidation/reduction peaks was also investigated by recording the cyclic voltammogram of the complex $\text{Mo}(\text{CO})_4(\text{BFEDA})$ at various scan rates (ranging from 0.05 to 1 V/s) (Figure 4.21). It is found that the oxidation potentials are shifted to more positive potentials and reduction peaks are shifted to more negative potentials upon increasing the voltage scan rate. In order to elucidate the mechanism of the processes on the electrode surface, peak current, I_p , versus square root of voltage scan rates was plotted and given in Figure 4.22. As seen from the figure, I_p increases linearly with the increasing voltage scan rate. This clearly indicates a diffusion control mechanism for the mass transport on the electrode surface.²¹

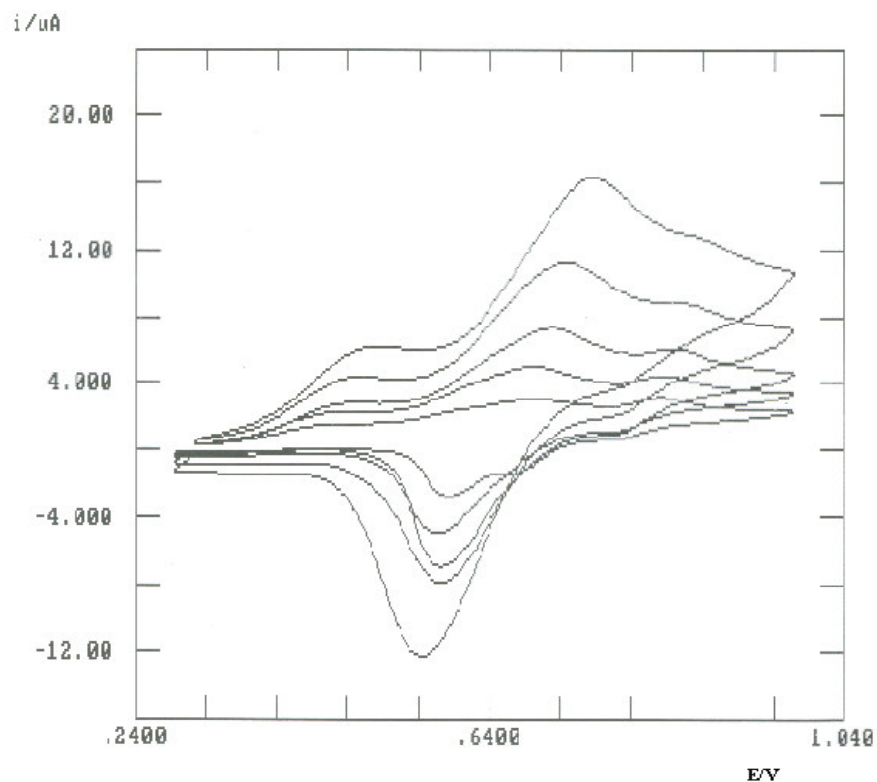


Figure 4.21. CV of $\text{Mo}(\text{CO})_4(\text{BFEDA})$ at scan rates of 50, 100, 200, 500 and 1000 mV/s in CH_2Cl_2 with reference electrode of Ag-wire.

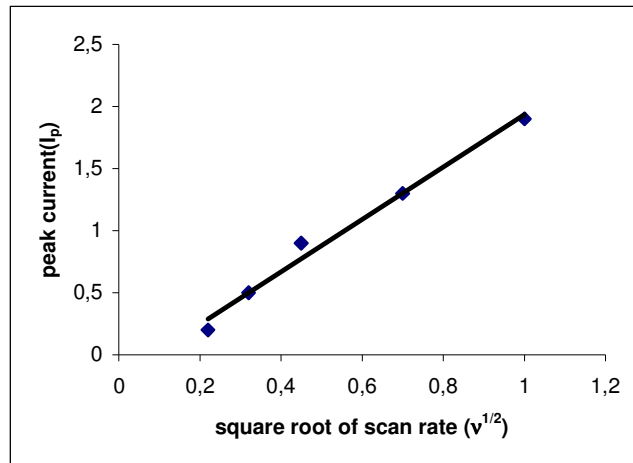


Figure 4.22. Graph of peak current (I_p) versus square root of scan rates ($v^{1/2}$) in cyclic voltammogram of $\text{Mo}(\text{CO})_4(\text{BFEDA})$.

The number of moles electron transferred in the oxidation of $\text{Mo}(\text{CO})_4(\text{BFEDA})$ complex was determined by chronoamperometry using the Ultra Micro Disc Electrode (UME) as follows:⁴⁶

The diffusion coefficient of the complex $\text{Mo}(\text{CO})_4(\text{BFEDA})$ can easily be determined by using chronoamperometrical Cottrel equation;

$$I_p = \frac{nFAD^{1/2}C}{(\pi t)^{1/2}} \quad (1)$$

Where;

I_p ; is the current density in chronoamperometric study (A).

n ; is the number of moles of electrons.

F ; is the Faraday constant which is 96485 C/mol.

A ; is the Surface area of electrode cm^2 .

D ; is the Diffusion coefficient (cm^2/s).

C ; is concentration (mol/cm^3).

t ; is the time (s).

A plot of I_p vs $t^{-1/2}$ gives a straight line, the slope of which is given by equation 2:

$$S = nFACD^{1/2}/\pi^{1/2} \quad (2)$$

It can be rearranged to give the number of moles of electrons n ;

$$n = \frac{S\pi^{1/2}}{FACD^{1/2}} \quad (3)$$

The same n value can also be obtained from Branski equation where;

I_{ss} ; is current density at long times.

The other variables are the same as reported above.

$$I_{ss} = 4rnFCD \quad (4)$$

It can also be rearranged to give number of moles of electrons n ;

$$n = \frac{I_{ss}}{4rFCD} \quad (5)$$

The two expressions for n are equalized to obtain the diffusion coefficient, D of $\text{Mo}(\text{CO})_4(\text{BFEDA})$.

The values of known variables for $\text{Mo}(\text{CO})_4(\text{BFEDA})$ complex is as follows;

Slope of the line (I_p versus $t^{1/2}$) = 6.48×10^{-10} ($\text{A}\cdot\text{s}^{-1/2}$)

$A = 3.14 \times 10^{-6}$ cm^2 from πr^2 where r equals to 0.001 cm

$I_{ss} = 1.19 \times 10^{-9}$ A from potentials between 0.7 - 1.3 V refer to SCE.

$C = 1.28 \times 10^{-6}$ mol/cm^3

Diffusion coefficient is found to be 6.62×10^{-7} cm^2/s from equations 3 and 5.

Than putting the D in equation 4, the number of moles of electrons in direction of oxidation (n) is found to be 3.64 mol electrons per mol of the compound.

The number of moles of electrons in the first oxidation could not be determined but from the current intensity in the voltammogram, it is estimated that one electron is transferred at the first oxidation. Moreover, if the half of the ΔE_p ($E_a - E_c/2$) is equal to 29 mV , number of moles of electrons transferred in oxidation is two; otherwise, the CV would reflect the overlap of two one-electron transfers.²¹ The half of the ΔE_p for last oxidation peak belonging to Mo center ($E_a = 0.83$ V , $E_c = 0.79$ V) in CV referred to Ag-wire is 29 mV .

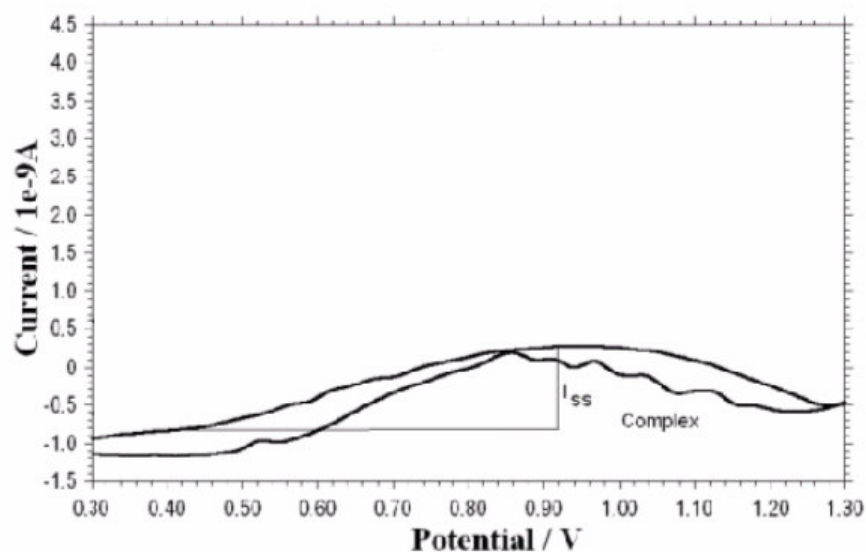


Figure 4.23. CV of $\text{Mo}(\text{CO})_4(\text{BFEDA})$ with UME electrode

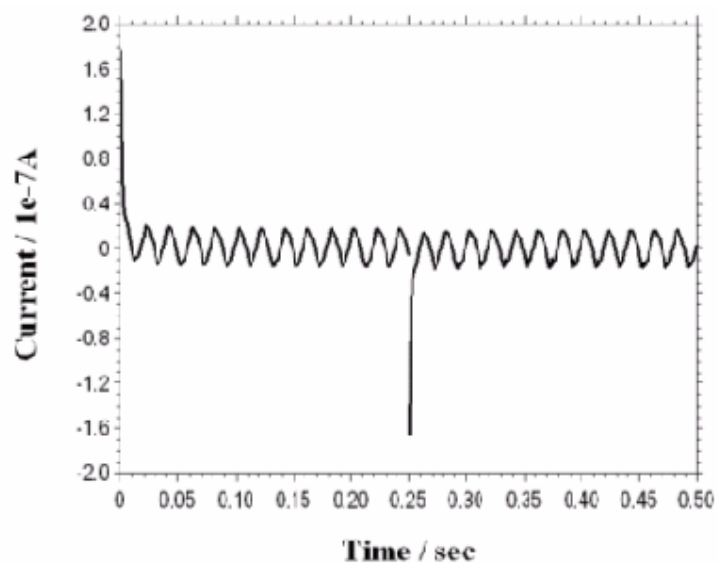


Figure 4.24. Chronoamperometric study of $\text{Mo}(\text{CO})_4(\text{BFEDA})$ using UME.

Controlled potential experiments both for the free BFEDA and the $\text{Mo}(\text{CO})_4(\text{BFEDA})$ complex were monitored by recording the changes in the UV-VIS spectrum of the solution. Potential was set to 650 mV during the controlled potential electrolysis of BFEDA (2×10^{-5} M). The continuous *in-situ* monitoring of

the changes revealed that the absorption bands of BFEDA shifts to lower energy as seen from Figure 4.25.

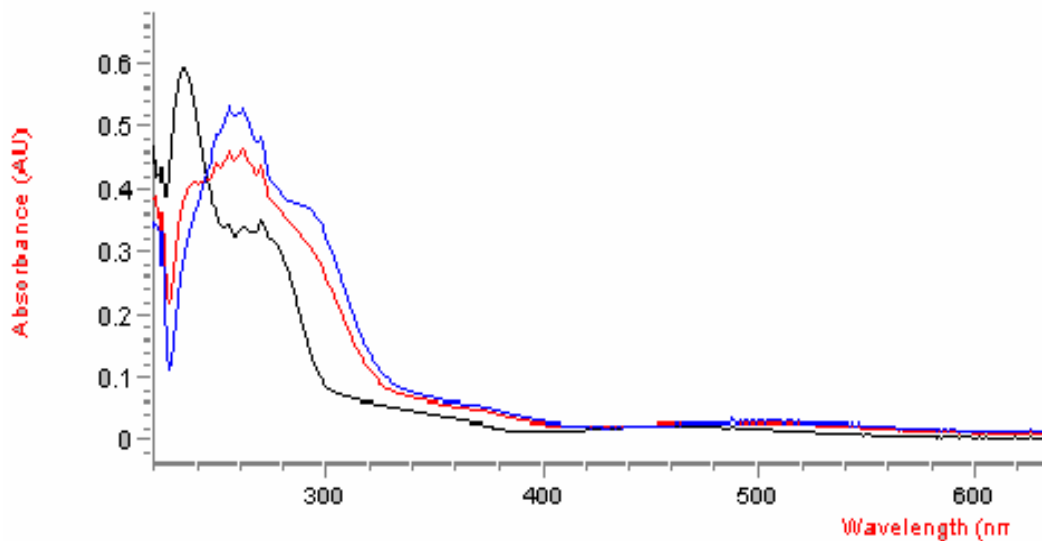


Figure 4.25. UV-VIS monitored controlled potential electrolysis of BFEDA in CH_2Cl_2 and 0.015 M TBATFB solution.

The UV-VIS spectrum of ferrocenium ion has four absorption bands as listed in Table 4.8. The comparison of absorption bands between free ferrocene and free ferrocenium cation are also seen in Table 4.8. The metal to ligand charge transfer transition energy increases if the positive charge of the central metal ion is increased. On the other hand, ligand to metal charge transfer transition energy decreases markedly with increasing positive charge of metal atom. Therefore, the absorption bands of ferrocenium cation at 198 and 250 nm have been reported to be metal to ligand charge transfer transition, whereas band at 283 nm has been assigned to be ligand to metal charge transfer transition. The bands at 380 and 523 nm have been reported to be d-d electron transition of Fe(III) , (d^5 ion).

Table 4.8. The absorption wavelengths (λ_{\max}) of free ferrocene and free ferrocenium ion in nm.

Ferrocene (Fe^{+2})	Ferrocenium (Fe^{+3})	Assignment
200	198	MLCT
265	250	MLCT
239	283	LMCT
324	380	d-d (Fe center)
458	523	d-d (Fe center)

The absorption bands of BFEDA^{+2} corresponding to the ferrocenium ion are 257, 293, 372, 520 nm. The band at 372 and 520 nm are the d-d electron transitions, whereas, the band at 257 and 293 nm are charge transfer transitions.

Recall that the first Mo center oxidation is an irreversible step to Mo(I). Since UV-VIS monitoring of the constant current electrolysis did not reveal any change other than ligand-based oxidation, the product of the first oxidation step is believed to be short-lived specie. This specie undergoes an intramolecular one- electron transfer and is reduced back to Mo(0) while ferrocene is oxidized to the ferrocenium cation at the same time. The constant current electrolysis of 5×10^{-5} M $\text{Mo}(\text{CO})_4(\text{BFEDA})$ solution was carried out at constant current of 100 mA. Until two electrons oxidation was completed, the trends in change of absorption bands are similar to BFEDA electrolysis and changes are continuous until two electrons oxidation was completed. Therefore, the electrolysis can be studied in two parts.

In the first part, two charge transfer transitions at 236 and 259 nm decrease in intensity and are slightly shifted to 238, 265 nm, respectively. The band at 304 nm which was assigned as d-d transition of Mo metal, is shifted to 296 nm while its intensity is increased. The band at 348 nm, which was assigned to be d-d transition of iron center, is decreased during electrolysis and a new band at 375 nm is formed. This new band is assigned to d-d transition of Fe^{+3} (d^5 ion). The absorption peak at

480 nm is shifted to 516 nm with increasing in intensity. Three isosbestic points can be seen in UV-VIS spectrum of the $\text{Mo}(\text{CO})_4(\text{BFEDA})$ complex. The observation of nice isosbestic points indicates a straightforward conversion of reactant into product without side or subsequent reaction. These changes are depicted in Figure 4.26.

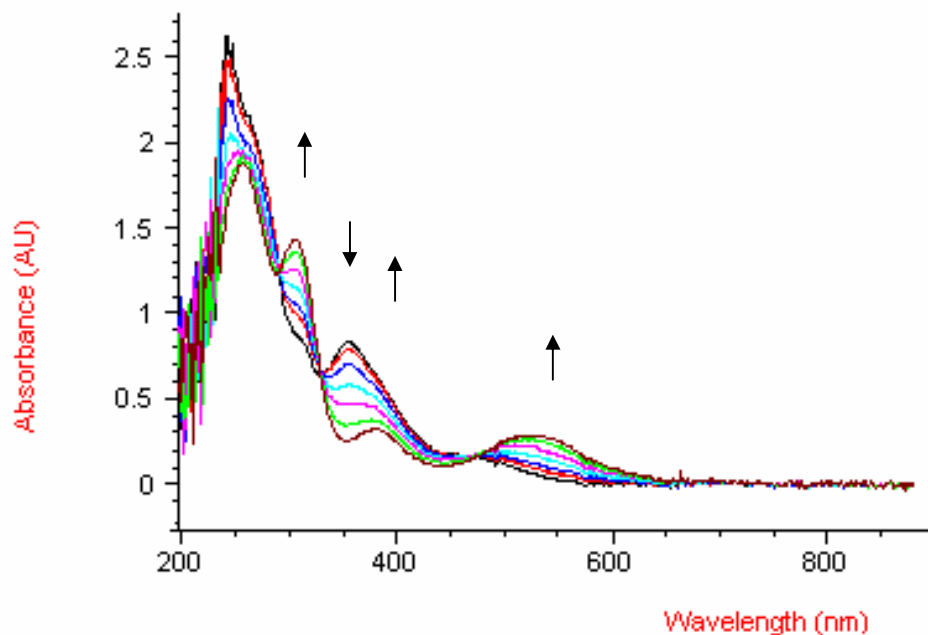


Figure 4.26. UV-VIS monitored constant current electrolysis of $\text{Mo}(\text{CO})_4(\text{BFEDA})$ in CH_2Cl_2 and TBATFB solution until two electron oxidations were completed.

In the second part, that is, after two-electron oxidation, trends in UV-VIS spectrum were changed because of molybdenum-centered oxidation (Figure 4.27). During electrolysis after two moles of electron passage, all absorption bands are decreased in intensity. More profound decrease is seen for absorption bands at 237, 267, 296 nm. The band at 375 and 516 nm is slightly decreased in intensity.

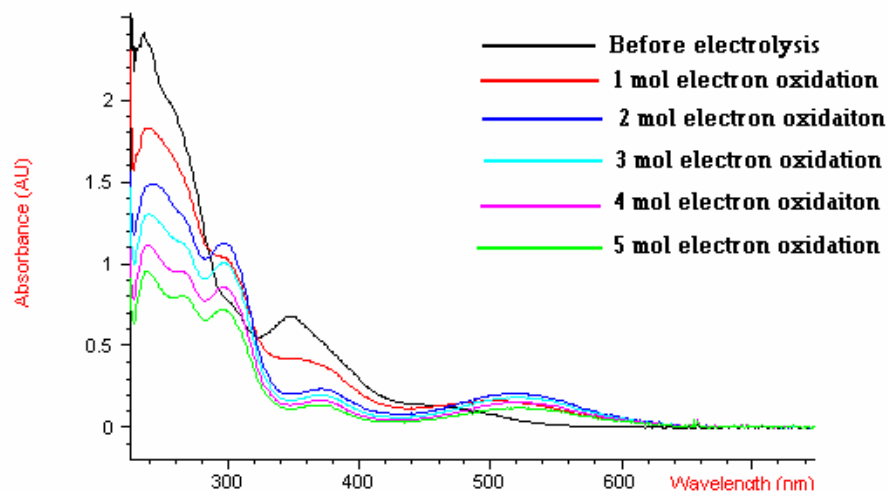


Figure 4.27. UV-VIS monitored controlled potential electrolysis of $\text{Mo}(\text{CO})_4(\text{BFEDA})$ in CH_2Cl_2 and TBATFB solution.

The spectral change continued until five moles of electron passage and Table 4.9 summarize all the changes during constant current electrolysis.

Table 4.9. Spectral change in UV-VIS of (a) BFEDA and (b) $\text{Mo}(\text{CO})_4(\text{BFEDA})$ during controlled potential electrolysis in CH_2Cl_2 and TBATFB solution.

Compound	CT	CT	d-d transition	d-d transition
BFEDA	234	267	346	460
BFEDA^+	258	291	371	505
BFEDA^{+2}	257	293	372	520

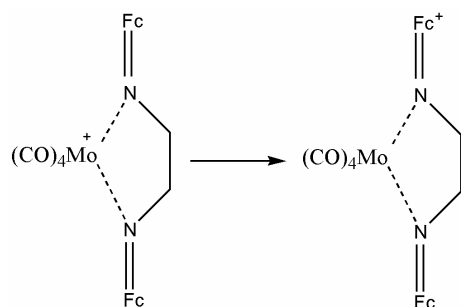
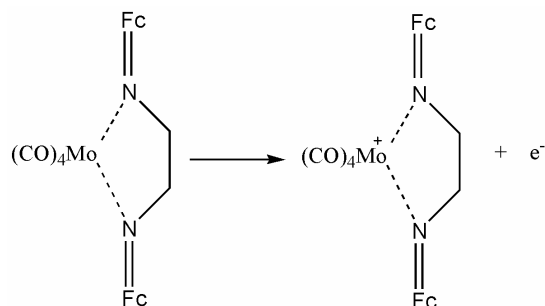
(a)

Compound	CT	CT	d-d transition (Mo)	d-d transition (Fe)	d-d transition (Fe)
$\text{Mo}(\text{CO})_4(\text{BFEDA})$	236	259	304	348	480
$\text{Mo}(\text{CO})_4(\text{BFEDA}^+)$	237	260	301	353	502
$\text{Mo}(\text{CO})_4(\text{BFEDA}^{+2})$	238	265	296	375	516
$\text{Mo}^+(\text{CO})_4(\text{BFEDA}^{+2})$	237	267	298	375	522
$\text{Mo}^{+3}(\text{CO})_4(\text{BFEDA}^{+2})$	237	267	300	372	524

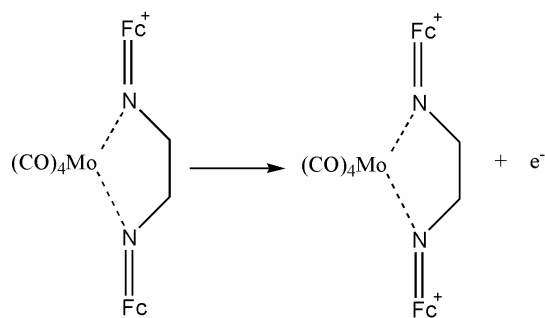
(b)

Thus from all the findings the following mechanism can be proposed for the oxidation of $\text{Mo}(\text{CO})_4(\text{BFEDA})$;

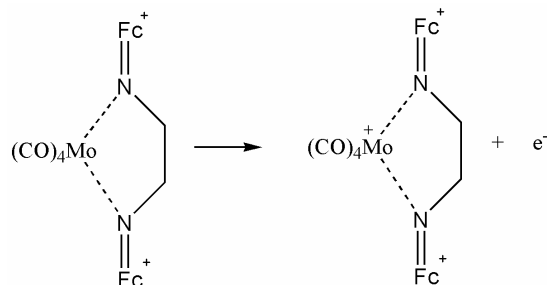
1. Oxidation of molybdenum fragment, changing the oxidation state of molybdenum from (0) to (+1), and then self reduction of molybdenum(+1) to molybdenum(0) by intramolecular electron transfer from iron(II) centers which is then oxidized to iron(III):



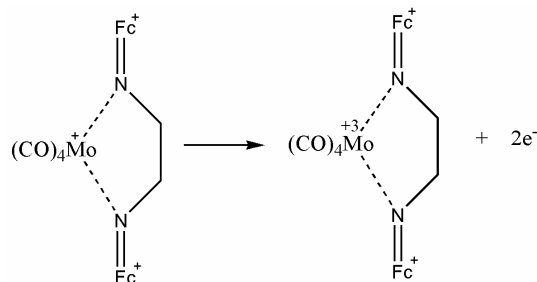
2. Oxidation of second ferrocene moiety, changing the oxidation state of iron center from (+2) to (+3):



3. Oxidation of molybdenum center, changing the oxidation state of molybdenum from (0) to (+1):



4. Oxidation of molybdenum center, changing the oxidation state of molybdenum from (+1) to (+3):



Electrochemical behavior of Mo(CO)₄(BFEDA) complex was also investigated by in-situ monitoring the changes in the FTIR spectrum of Mo(CO)₄(BFEDA) in CH₂Cl₂ solution during cyclic voltammetric studies. This was achieved by using a one-compartment cell. It was observed that while absorption bands of Mo(CO)₄(BFEDA) are decreasing in intensity, two new absorption bands are seen at 1982 and 1712 cm⁻¹ which belongs to Mo(CO)₆ and a kind of bridging carbonyl, respectively (Figure 4.28). Although, this result, indicating the decomposition of Mo(CO)₄(BFEDA) complex to hexacarbonylmolybdenum(0), is different from what we have found from in-situ UV-VIS studies, the comparison is not possible because of the differences in conditions of two experiments.

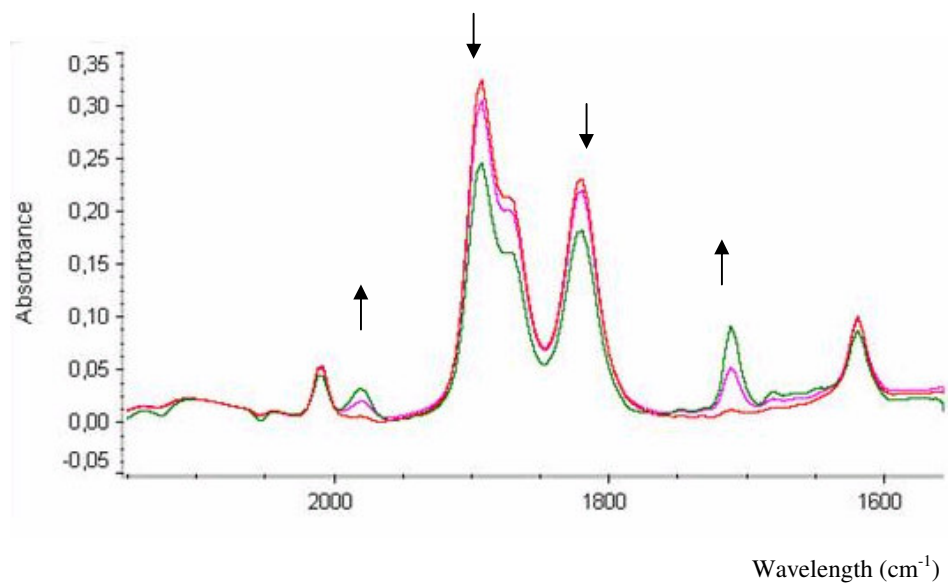


Figure 4.28. FTIR spectra during electrolysis of 1×10^{-4} M $\text{Mo}(\text{CO})_4(\text{BFEDA})$ in CH_2Cl_2 and 0.1 M TBATFB solution at constant current.

CHAPTER 5

CONCLUSIONS

The N,N'-bis(ferrocenylmethylene)ethylenediamine (BFEDA) was prepared from the reaction of ferrocenecarboxaldehyde and ethylenediamine in benzene solution by using a Dean-Stark apparatus and characterized by IR, Raman and NMR spectroscopies. This diimine molecule containing two ferrocenyl moieties was employed as a bidentate ligand in the synthesis of tetracarbonyl [N,N'-bis(ferrocenylmethylene)ethylenediamine]molybdenum(0), Mo(CO)₄(BFEDA).

The Mo(CO)₄(BFEDA) was synthesized and isolated for the first time from the ligand exchange reaction of tetracarbonyl(bicyclo[2.1.1]hepta-2,5-diene)molybdenum(0) with N,N'-bis(ferrocenylmethylene)ethylenediamine (BFEDA) in toluene solution. The reaction of tetracarbonyl($\eta^{2:2}$ -1,5-cyclooctadiene)molybdenum(0) and BFEDA also gives the same complex Mo(CO)₄(BFEDA).

Mo(CO)₄(BFEDA) was fully characterized by elemental analysis, UV-VIS, IR, ¹H-NMR, ¹³C-{¹H}-NMR and Mass spectroscopies. The IR spectrum of Mo(CO)₄(BFEDA) displays four CO stretching bands due to C_{2v} local symmetry and one C=N stretching band. The C_{2v} symmetry of Mo(CO)₄ fragment was also confirmed by ¹H-NMR and ¹³C-{¹H}-NMR spectroscopies.

IR and ¹³C-{¹H}-NMR spectra show that BFEDA molecule is a σ -donor ligand rather than a π -acceptor ligand. This σ -donation ability of BFEDA upon coordination causes a decrease in the electron density of all the atoms in the BFEDA fragment except ipso carbons of substituted cyclopentadienyl ring of ferrocene

moieties. Another consequence of the σ -donation from BFEDA to $\text{Mo}(\text{CO})_4$ fragment is the weakening of the $\text{C}\equiv\text{O}$ triple bond of the carbonyl groups due to the enhanced metal $\rightarrow\text{CO}$ back bonding.

The electrochemical behavior of $\text{Mo}(\text{CO})_4(\text{BFEDA})$ was also studied by using cyclic voltammetry and differential pulse voltammetry. Mechanism of the electrode reaction was investigated by in-situ UV-VIS and IR spectroscopic measurements during the electrolysis. Moreover, chronoamperometry was performed to determine the number of moles of electrons transferred in the direction of oxidation.

The most important outcome emerging from this study is that the complex $\text{Mo}(\text{CO})_4(\text{BFEDA})$ has three redox active centers, one molybdenum and two iron, communicating with each other electronically via π conjugation. According to the results of the electrochemical studies, molybdenum metal is oxidized first in cyclic voltammetry. Next, the ferrocene centers undergo subsequent one-electron oxidations from $\text{Fe}(\text{II})$ to $\text{Fe}(\text{III})$ and, finally, molybdenum undergoes a two-electron oxidation from $\text{Mo}(\text{I})$ to $\text{Mo}(\text{III})$. In the electrolysis, an intramolecular electron transfer occurs from one iron to molybdenum, reducing the molybdenum from $\text{Mo}(\text{I})$ back to $\text{Mo}(\text{0})$.

REFERENCES

1. Mathey, F.; Sevin, A., *Molecular Chemistry of the Transition Elements*; John Wiley & sons, England, **1988**.
2. Komiya, S., *Synthesis of Organometallic Compounds*, John Wiley & sons. New York, **1997**.
3. Huheey, J.E.; Keiter, R.L., *Inorganic Chemistry-Principles of Structure and Reactivity, 4th Ed.*, Harpercollins College Publishers, New York, **1993**.
4. Cotton F.A., *Advanced Inorganic Chem*; York, **1988**.
5. Crabtree, R.H.; Wilkinson, G., *Advanced Inorganic Chemistry 5th edition*, John Wiley & sons Inc., New York, **1988**.
6. Constable; E.C., *Metals and Ligand Reactivity*, Ellis Horwood limited, England, **1990**.
7. Elschenbroich, C.; Salzer A., *Organometallics, 2nd Ed.*, VCH, Weinhiem, **1992**.
8. Caubet, A.; Lopez, C.; Bosque, R.; Solans, X.; Bardia-Font, M., *J. Organometallics Chemistry*, **577**, 292, **1999**.
9. Yaman, G., Master Dissertation, Middle East Technical University, Department of Chemistry, **2002**.
10. Ozkar, S.; Kayran, C.; Demir, N., *J. Organometallics Chemistry*, **688** , 62, **2003**.
11. Hongyun, Z.; Feng, Li; Peikun, C.; Deji, C.; Dongli, C.; Hongquan, Z., *Polyhedron*, **12**, 165, **1993**.
12. Elschenbroich, C.; Salzer, A., *Organometallics, 2nd Ed.*, VCH, Weinhiem, **1992**.
13. DuBois, D.L.; Elgenbrot, W, *Organometallics*, **5**, 1405, **1986**.
14. Coleman, K.S.; Turberville, S.; Pascu, S.I.; Green, M.L., *J. Organometallic Chemistry*, **689**, 770, **2004**.
15. Togni, A.; Hayashi, T. Eds., *Ferrocenes*; VCH, Weinheim, **1995**

16. Akyol, C., Master Dissertation, Middle East Technical University, Department of Chemistry, **2005**
17. Fisher, E. O.; Fröhlich, W., *Chem. Ber.*, **92**, 2995, **1959**.
18. King, R.B.; Fronzaglia, A., *Inorganic Chemistry.*, **5**, 1837, **1966**.
19. Pickett, C.J.; Pletcher, D., *J.C.S. Chem. Comm.*, 6608, **1974**
20. Connely, N.G.; Geiger, W.E., *Advances in Organometallic Chemistry*, Academic Press, New York, **23**, 1 , **1984**.
21. Gosser, D. K., *Cyclic Voltammetry*, VCH Verlagsgesellschaft, USA, **1993**.
22. Shultz, F.A.; Ott, V.R.; Rollison, D.S.; Brovard, D.C.; McDonald, J.W., Newton W.E., *Inorg. Chem.*, **17**, 1758, **1978**.
23. Shriver, D.F.; Atkins, P.W., Langford S.H., *Inorganic Chemistry 2nd edition*, Oxford University press, Oxford, **1994**.
24. Constable, E. C., *Metal and Ligand Reactivity*, VCH Verlagsgesellschaft, Weinheim, Germany; **1996**.
25. Werner, H.; Prinz, R., *Chem. Ber.*, **100**, 265, **1967**.
26. (a) Neuse, E.W.; Meirim, M. G.; Blom, N.F., *Organometallics*, **7**, 2562; **1988**.
(b) Bracci, M.; Ercolani, C.; Floris, B.; Bassetti, M.; Chiesi-Villa, A., *J.Chem.Soc., Dalton Trans.* , 1357, **1990**.
27. Benito, A.; Cano, J.; Martinez-Manez, R.; Santo, J.; Paya, J.; Lloret, F.; Julve, M.; Faus, J.; Marcos, D., *Inorganic Chemistry*, **32**, 117, **1993**.
28. Graham, P.J.; Lindsey, R.V.; Parshall, G.W.; Peterson, M.L; Whitman, G.M., *J.Am.Chem.Soc.*, **79**, 3416, **1957**.
29. Braterman, P.S., *Metal Carbonyl Spectra*, Academic Press, London, **1975**.
30. Jones, R.A.; Lopez-Quintanilla G.; Taheri S.A.N.; Hania M.M.; Öztürk O.; Zuilhof H., *J. Chem. Research, Synopses*, **8**, 835, **2001**.
31. Pickett, T.E.; Richards, C.J., *Tetrahedron Letters*, **40**, 5251, **1999**.
32. Marie-Madeleine, Rohmer, *Chemical Physics Letters*, **29**, 466, **1974**.
33. Cotton, F.A.; Kraihanzel, C.S.; *J.Am. Chem.Soc.*, **84**, 4432, **1962**.
34. Mukerjee, S.L.; Nolan, S.N.; Hoff, C.D., *Inorg.Chem.*, **27**, 85, **1988**.

35. Orgel, L.E., *Inorg. Chem.*, **1**, 25, **1962**.
36. Braianga, J.; *J.of Mol.Struc.*, **570**, 109, **2001**.
37. Hyde, C. L.; Darensbourg, D. J., *Inorg. Chem.*, **12**, 1075, **1973**.
38. Mukerjee, S.; Nolan, S.; Hoff, C.; Vega, R., *Inorg. Chem.*; **27**, 81, **1988**.
39. Campbell, T.; Alexander, M. G.; Hart, R.; Orchard, S. D.; Pope, S. J.A.; Reid, G., *J. Organometallic Chem.*, **592**, 296, **1999**.
40. Bodner, G., *Inorg. Chem.*, **14**, 2694, **1975**.
41. Gao, Y.; Shi, Q.; Kershner, D.; Basolo, F., *Inorg. Chem.*, **27**, 188, **1988**.
42. (a) Schreimer, G.E., *Inorg. Chem.*, **21**, 3575, **1982**.
(b) Rawling, K.A.; Lees, A.J., *Inorg. Chem.*, **28**, 2154, **1989**.
(c) Lees, A.J., *J. Am Chem. Soc.*, **104**, 2038, **1982**.
(d) Servaas, P.C.; Dijk, H.K.; Snoeck, T.C.; Stufkens, D.J; Oskam, A., *Inorg Chem.*, **24**, 4494, **1985**.
43. Crutchley, R.J.; Lever, A. B.P., *Inorg. Chem.*, **21**, 2277, **1982**.
44. (a) Wong, W.Y.; Cheung, S.H.; Loe, S.M.; Leung, S.Y., *J. Organomet. Chem.*, **596**, 36, **2000**.
(b) Kühn, F.E.; Goncalves, I.S.; Lopes, A.D.; Lopes, J.P.; Romao, C.; Wachter, W.; Mink, J.; Hajba, L.; Parola, A.J.; Pina, F.; Sotomayor, J., *Eur. J. Inorg. Chem.*, 295, **1999**.
45. Bildstein, B.; Malaun, M.; Kopacka, H.; Fontani, M.; Zanello, P., *Inorg. Chimica Acta*, **300**, 16, **2000**.
46. (a) Baranski, A.S.; Fawcett, W.R.; Gilbert, C.M., *Anal Chem*, **57**, 166, **1985**.
(b) Aoki, K; Osteryoung, J., *J. Electroanal. Chem.*, 43, **1989**.

APPENDIX

UV-VIS spectra of 2.5×10^{-5} , 5.0×10^{-5} , 7.5×10^{-5} M free BFEDA molecule was taken in CH_2Cl_2 solution at room temperature.

Wavelength	Molar Absorbivity L/mole.cm
234	29650
267	16500
346	2750
460	1050

UV-VIS spectra of 2.5×10^{-5} , 5.0×10^{-5} , 7.5×10^{-5} M $\text{Mo}(\text{CO})_4(\text{BFEDA})$ molecule was taken in CH_2Cl_2 solution at room temperature.

Wavelength	Molar Absorbivity L/mole.cm
236	47760
260	36840
304	14140
350	12479
461	2417